Inorganic Chemistry

pubs.acs.org/IC Article

Alternative Route Triggering Multistep Spin Crossover with Hysteresis in an Iron(II) Family Mediated by Flexible Anion Ordering

Hiroaki Hagiwara,* Ryo Minoura, Taro Udagawa, Ko Mibu, and Jun Okabayashi

Cite This: https://dx.doi.org/10.1021/acs.inorgchem.0c01069 Read Online

ACCESS | Metrics & More | Article Recommendations | Supporting Information

ABSTRACT: Multistep spin crossover (SCO) compounds have attracted much attention, since they can be great candidates for high-density multinary memory devices. The introduction of substituents, such as methyl (Me), chloro (Cl), bromo (Br), and methoxy (MeO) groups, at para positions to the phenyl-substituted tripodal N_6 ligand-coordinated SCO Fe^{II} material, $[FeL^{Ph}](NTf_2)_2$ [where L^{Ph} = tris(2-{[(1-phenyl-1*H*-1,2,3-triazol-4-yl)methylidene]amino}ethyl)amine and NTf_2 = bis(trifluoromethanesulfonyl)imide], affords a new family of solvent-free Fe^{II} complexes: $[FeL^{4\text{-R-Ph}}](NTf_2)_2$ {where $L^{4\text{-R-Ph}}$ = tris[2-({[1-(4-R-phenyl)-1*H*-1,2,3-triazol-4-yl]methylidene}amino)ethyl]amine, where R = Me (**1**), Cl (**2**), Br (**3**), and MeO (**4**)}. **1** shows temperature invariant high-spin (HS) state, whereas the others show spin transitions with different characteristics, such as half-SCO (**4**), two-step SCO (**3**), and unusual three-step SCO with hysteresis (**2**). Mössbauer and X-ray absorption fine structure (XAFS) spectroscopic studies of them support the magnetic susceptibilities results. Density functional theory calculations indicate that the electronic effect of different substituents on magnetic properties is negligible in this Fe^{II} family. Single-crystal X-ray diffraction studies reveal that **1**−**4** has a similar packing arrangement with three-dimensional supramolecular network via intermolecular $\pi-\pi$ and CH···π interactions between complex cations, and CH···X (X = O, N, and F) hydrogen bonding interactions between cations and inherently frustrated NTf_2 anions. Variable-temperature structural studies unveil a variety of stepped SCO behaviors of **2**−**4** and deactivation of SCO in **1** are governed by the regulation of ordering of NTf_2 counteranions through the subtle modification of terminal substituents of complex cations. Quantitative light-induced excited spin-state trapping (LIESST) effect was observed for **2**−**4** via green light irradiation (532 nm) at 10 K. This study opens up a new way for systematic control of magnetic response from no SCO to half-, two-step, and finally three-step SCO with hysteresis by precise tuning of the ordering of flexible NTf_2 anions included in the supramolecular network with potentially SCO-active complex cations.

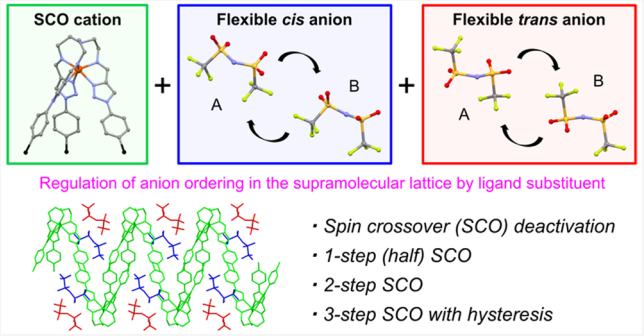

INTRODUCTION

Spin crossover (SCO) is one of the most intriguing properties of molecular-based switching materials.[1−3] Two distinct spin states of SCO complexes [i.e., high-spin (HS) and low-spin (LS) states] can be accessible by external stimuli, such as temperature, pressure, light, or magnetic field. SCO compounds are also known to exhibit not only one-step LS↔HS conversion but also stepped SCO with various thermal dependencies, such as gradual, abrupt, hysteretic, or a complex combination of them.[4,5] Abruptness and hysteresis of spin transition are brought by cooperativity between SCO sites through the utilization of bridging ligands in polymeric systems[6,7] and intermolecular interactions in supramolecular systems.[8−10]

In addition to the demands for exploring SCO compounds having wide thermal hysteresis at around room temperature (RT) for potential applications in data storages, sensors, and display devices,[11,12] multistep SCO materials have also attracted much attention, since their novel electronic functionalities are worth exploring for practical application in high-density memories. From the theoretical point of view, two-dimensional (2D)[13,14] and one-dimensional (1D)[15] elastic frustration models have been reported for understanding the emergence of multistep SCO (with hysteresis), depending on the strength of the elastic frustration arising from antagonistic solid-state interactions. Along this line, 2D Hofmann-type materials have been developed for exhibiting stepped SCO.[16,17] Moreover, four-step SCO have recently been achieved in various 2D and three-dimensional (3D) coordination polymers.[18−23] Stepped SCO is also observed in discrete

Received: April 13, 2020

https://dx.doi.org/10.1021/acs.inorgchem.0c01069
Inorg. Chem. XXXX, XXX, XXX−XXX

polynuclear systems having two[24] or more potentially SCO-active metal sites.[25,26] Interestingly, one tetranuclear mixed-valence iron grid-like complex exhibits site-selective spin-state switching using different laser-light stimuli.[27]

In mononuclear system, stepwise SCO is achieved by chemical modifications of ligand substituents, counteranions, and crystal solvents. For example, well-known ligand systems, such as $[Fe^{II}(2\text{-pic})_3]Cl_2$·solvent,[28] $[Fe^{II}(tpa)(NCS)_2]$·solvent,[29] and $[Fe^{III}(qsal\text{-}I)_2]OTf$·solvent[30] [where 2-pic = 2-picolylamine, tpa = tri(2-pyridylmethyl)amine, and qsal-I = 5-iodo-*N*-(8-quinolyl)salicylaldimine], show solvent-dependent stepwise SCO. The qsal-X ligand system also shows the substituent-dependent stepped SCO in a halogenated Fe^{II} family, $[Fe^{II}(qsal\text{-}X)_2]$.[31,32] Alkyl substituents of the imidazole-containing bidentate ligand family, *fac*-$[Fe^{II}(HL^R)_3]Cl$·PF_6 {HL^R = [(2-methylimidazol-4-yl)methylidene]-monoalkylamine}, exhibit a drastic effect to change SCO profile, reaching three-step SCO in the *n*-hexyl derivative.[33,34] Other imidazole-based systems such as hexadentate $[Fe^{II}H_3L^{Me}]Cl$·X[35] and tridentate $[Fe^{II}(H_2L^{2\text{-}Me})_2]X$·Y[36] [$H_3L^{Me}$ = tris(2-{[(2-methylimidazol-4-yl)methylidene]-amino}ethyl)amine, $H_2L^{2\text{-}Me}$ = [(2-methylimidazol-4-yl)-methylidene]histamine], show two-step SCO with a moderate or wide plateau region, depending on the anion size (X or Y). A four-step SCO compound has been synthesized by the combination of the known SCO cation, $[Fe^{II}(dpp)_2]^{2+}$ [dpp = 2,6-bis(pyrazol-1-yl)pyridine], and the magnetically bistable anion, $[Ni(mnt)_2]^-$ (mnt = maleonitriledithiolate), instead of commonly used counteranions.[37] This deliberate combining of bistable components with SCO molecules is a new effective strategy for the development of multistep SCO materials.

Recently, the bis(trifluoromethanesulfonyl)imide (NTf_2) anion has attracted much attention, since it is a useful component for the synthesis of ionic liquids by utilizing its conformational flexibility arising from its rotational freedom. In the SCO research, Mochida et al. have reported a first SCO ionic liquid in 2013, by the combination of the SCO Fe^{III} cation and the NTf_2 anion.[38] In 2014, we have reported a first SCO Fe^{II} solid containing two NTf_2 anions, $[FeL^{Ph}](NTf_2)_2$ [where L^{Ph} = tris(2-{[(1-phenyl-1*H*-1,2,3-triazol-4-yl)-methylidene]amino}ethyl)amine] (see Chart 1).[39] It shows an one-step LS ↔ HS SCO at around RT ($T_{1/2}$ = 280 K) with order−disorder transition of the NTf_2 anion from the low-temperature ordered *trans*- (*anti*-) conformer to the disordered mixture of *cis*- (*syn*-) and *trans*-conformers at RT (Chart 1b). After that, two-step SCO (with hysteresis) was achieved by order−disorder transition of the NTf_2 anion in a Mn^{III} compound by Morgan et al. in 2015,[40] and abrupt SCO near RT with 34 K hysteresis was exhibited by conformational change of ordered NTf_2 anion in an Fe^{III} system.[41] In this system, the NTf_2 anion has an intermediate conformation between the *syn*- and *anti*-conformers in the LS state. Thus, the NTf_2 anion has at least three conformers and disordered form of them in the crystal lattice and can behave as a multistable component. In this way, interesting SCO properties related to flexible NTf_2 anion have been sporadically reported over the past few years in Fe^{II}, Fe^{III}, and Mn^{III} complexes. However, rational control of this anion flexibility for showing on-demand spin state switching has never been achieved.

The above-mentioned SCO Fe^{II} complex $[FeL^{Ph}](NTf_2)_2$ has the 3D network through $\pi-\pi$ and CH···π interactions between neighboring complex cations and multiple CH···X (X = N, O, and F) hydrogen bonding interactions between

Chart 1. Structures of $[FeL^{4\text{-}R\text{-}Ph}]^{2+}$ (R = H, for the Compound in ref 39; Me, Cl, Br, and MeO for 1, 2, 3, and 4, respectively) and NTf_2 Anion. (b) Two Conformers (*cis* and *trans*) of the NTf_2 Anion

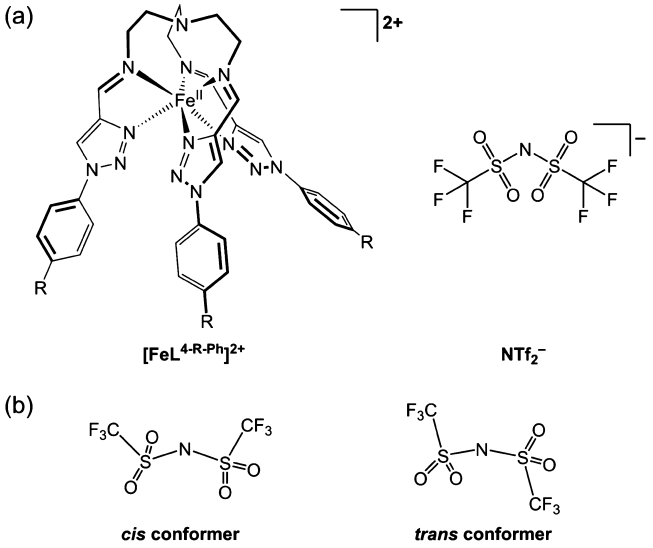

complex cations and NTf_2 anions. This 3D supramolecular network has the potential to accommodate both cooperativity between SCO metal sites and elastic frustration arising from the antagonistic cation···cation and cation···conformationally flexible NTf_2 anion interactions via steric effects or multiple intermolecular CH···X contacts. Thus, control of the ordering of NTf_2 anions by subtle modification possibly leads to a variety of SCO behaviors in the Fe^{II} system. So, in this work, we introduce small substituents such as methyl (Me), chloro (Cl), bromo (Br), and methoxy (MeO) groups into the para-positions of phenyl groups of $[FeL^{Ph}](NTf_2)_2$ as the furthermost substituents from the metal center, to avoid a significant electronic impact on the Fe^{II} ion while, at the same time, providing strong impact on the cation-to-cation and cation-to-anion packing interactions. Here, we report an unprecedented route triggering multistep SCO with hysteresis through strategical regulation of flexible anion ordering related to the substituent modifications by the comprehensive study of a new Fe^{II} family, $[FeL^{4\text{-}R\text{-}Ph}](NTf_2)_2$ {where $L^{4\text{-}R\text{-}Ph}$ = tris[2-({[1-(4-R-phenyl)-1*H*-1,2,3-triazol-4-yl]methylidene}amino)-ethyl]amine, where R = Me (**1**), Cl (**2**), Br (**3**), and MeO (**4**)}, including temperature dependencies of magnetic susceptibilities, Mössbauer and X-ray absorption fine structure (XAFS) spectra, crystal structures, differential scanning calorimetry (DSC), and density functional theory (DFT) calculations. The effective photomagnetic responses (light-induced excited spin-state trapping, hereafter abbreviated as LIESST)[42] of this family are also reported.

RESULTS AND DISCUSSION

Synthesis and Characterization. All the synthetic procedures were performed in air (see the Supporting Information). The ligand precursor, 1-(4-R-phenyl)-*1H*-1,2,3-triazole-4-carbaldehyde (R = Me, Cl, Br, and MeO), was synthesized through general three step syntheses using commercially available reagents, i.e., (1) azidation of 4-substituted aniline,[43,44] (2) azide−alkyne click reaction of 4-R-phenyl azide and 2-propyn-1-ol,[43,44] and (3) MnO_2

https://dx.doi.org/10.1021/acs.inorgchem.0c01069
Inorg. Chem. XXXX, XXX, XXX−XXX

Table 1. Crystallographic Data for 1, 2, 3, and 4 at 296 K

complex	$[FeL^{4\text{-Me-Ph}}](NTf_2)_2$, **1**	$[FeL^{4\text{-Cl-Ph}}](NTf_2)_2$, **2**	$[FeL^{4\text{-Br-Ph}}](NTf_2)_2$, **3**	$[FeL^{4\text{-MeO-Ph}}](NTf_2)_2$, **4**
formula	$C_{40}H_{39}F_{12}FeN_{15}O_8S_4$	$C_{37}H_{30}Cl_3F_{12}FeN_{15}O_8S_4$	$C_{37}H_{30}Br_3F_{12}FeN_{15}O_8S_4$	$C_{40}H_{39}F_{12}FeN_{15}O_{11}S_4$
formula weight	1269.95	1331.20	1464.58	1317.95
crystal system	monoclinic	monoclinic	monoclinic	triclinic
space group	$P2_1/c$ (No. 14)	$P2_1/c$ (No. 14)	$P2_1/c$ (No. 14)	$P\bar{1}$ (No. 2)
a, Å	13.3124(3)	13.4137(3)	13.6483(5)	13.0485(3)
b, Å	13.8064(2)	13.8364(6)	13.8954(5)	13.5488(2)
c, Å	30.0553(8)	29.1300(11)	28.9747(9)	31.7970(5)
α, deg	90	90	90	90.0901(14)
β, deg	100.024(2)	98.669(3)	98.496(3)	91.7726(15)
γ, deg	90	90	90	93.6286(16)
V, Å^3	5439.7(2)	5344.7(3)	5434.7(3)	5607.45(18)
Z	4	4	4	4
d calcd, g cm^{-3}	1.551	1.654	1.790	1.561
μ, mm^{-1}	0.535	0.694	2.740	0.526
R_1,[a] wR_2[b] ($I > 2\sigma(I)$)	0.0648, 0.1880	0.0763, 0.2116	0.0678, 0.1842	0.0911, 0.2209
R_1,[a] wR_2[b] (all data)	0.0958, 0.2175	0.1072, 0.2433	0.1067, 0.2138	0.1204, 0.2443

[a] $R_1 = \sum||F_o| - |F_c||/\Sigma|Fo|$. [b] $wR_2 = [\sum w(|F_o|^2 - |Fc|^2)^2/\sum w(|F_o|^2)^2]^{1/2}$.

oxidation of alcohol to aldehyde.[43−45] The tripodal hexadentate ligand, abbreviated as $L^{4\text{-R-Ph}}$, was prepared by the 3:1 condensation reaction of 1-(4-R-phenyl)-*1H*-1,2,3-triazole-4-carbaldehyde and tris(2-aminoethyl)amine in CH_2Cl_2 (for **2**−**4**) or CH_2Cl_2/MeOH mixed solution (for **1**), and the resulting ligand solution was used for the syntheses of Fe^{II} complexes without isolation and purification. The complexes were prepared by mixing the ligand, $Fe^{II}Cl_2{\cdot}4H_2O$, and $LiNTf_2$ in a 1:1:2 molar ratio in CH_2Cl_2/MeOH mixed solution, evaporation of the solvent, addition of water to residual oil, extraction of it in CH_2Cl_2 and re-evaporation of it, and recrystallization of the residual from EtOH (for **1**) or MeOH (for **2**−**4**). All complexes were obtained as orange block crystals with the formula of $[Fe^{II}L^{4\text{-R-Ph}}](NTf_2)_2$ (no lattice solvents) confirmed by elemental analyses and thermogravimetric analysis (TGA) (see Figure S1 in the Supporting Information). The infrared (IR) spectra of **1**−**4** at RT showed a characteristic band at ca. 1650 cm^{-1} corresponding to the C═N stretching vibration of the Schiff-base ligand (Figure S2 in the Supporting Information).[39,46] The spectra also showed the strong bands assignable to the O═S═O vibrations at ca. 1349 and 1136 cm^{-1} and the C−F vibration at ca. 1198 cm^{-1} of NTf_2 anions.[39]

Structural Description at 296 K. Single-crystal X-ray diffraction (XRD) studies were performed for **1**−**4** at 296 K. The crystallographic data are summarized in Table 1 (and also Tables S1−S4 in the Supporting Information). Selected structural parameters for the complexes are given in Table 2 (detailed coordination bond lengths and angles are also given in Tables S5−S8 in the Supporting Information). The complexes **1**−**4** are isostructural. Indeed **1**−**3** are isomorphous, with the monoclinic space group $P2_1/c$, and the crystallographic unique unit of them consists of one complex cation, $[Fe^{II}L^{4\text{-R-Ph}}]^{2+}$, and two NTf_2 anions in which the two anions are both *cis* and *trans* conformers with or without disorder (see Table 1, as well as Table S9 in the Supporting Information). While **4** crystallized in the triclinic space group $P\bar{1}$, the unit-cell parameters are actually very similar to those for monoclinic **1**−**3** (see Table 1), and the two cations in the asymmetric unit of **4** are isostructural with those of **1**−**3** (see Table 2).

Figure 1 shows the molecular structures of **1**−**3** at 296 K. The Fe^{II} ion have an octahedral coordination environment

Table 2. Selected Structural Parameters for 1, 2, 3, and 4 at 296 K

complex	1	2	3	4	
metal site				Fe1	Fe2
spin state	HS	HS	HS	HS	HS
Complex Cation					
average Fe−N, Å	2.210	2.209	2.204	2.214	2.204
Σ,[a] deg	131.8	133.9	132.8	135.6	130.3
Θ,[b] deg	232.0	231.8	228.9	241.0	228.2
S(Oh)[c]	2.696	2.707	2.649	2.762	2.635
V_{Oh}, Å^3	13.219	13.194	13.123	13.327	13.135
Occupancies of Anions					
cis A	0	0.466	0.570	0	0
cis B	1	0.534	0.430	1	1 (inverted)
trans A	1	1	0.749	1	1
trans B	0	0	0.251	0	0

[a] Σ is the sum of $|90 - \phi|$ for the 12 *cis* N−Fe−N angles in the octahedral coordination sphere.[47] [b] Θ is the sum of $|60 - \theta|$ for the 24 N−Fe−N angles describing the trigonal twist angles.[48] [c] Continuous shape measures (CShM's). The reference shape is the regular octahedron with center.[49]

with the N_6 donor ligand corresponding to three Fe−N_{imine} and three Fe−$N_{triazole}$ bonds of the tripodal hexadentate Schiff-base ligand $L^{4\text{-R-Ph}}$. The complex cation is a chiral species with Δ- or Λ-isomers (Δ-isomers are indicated in Figure 1). The average Fe−N bond distances (here after abbreviated as Fe−N_{ave}) of **1**−**3** at 296 K are similar values (2.210, 2.209, and 2.204 Å, respectively), indicating that **1**−**3** are assignable to the Fe^{II} HS state. The octahedral distortion parameters Σ and Θ,[47,48] continuous shape measures (CShM's) S(Oh),[49] and octahedral volume (hereafter abbreviated as V_{Oh}) have no remarkable difference among **1**−**3**, showing the equivalence of their coordination spheres (Table 2). On the other hand, while NTf_2 counteranions exist in the same position of the lattice among **1**−**3**, their conformational arrangements are different to each other (Figure 1 and Table 2). In the lattice, they possibly have two types of *cis* NTf_2 conformers (distinguished as *cis* A and *cis* B) and two types of *trans* conformers (distinguished as *trans* A and *trans* B), and **1** contains only *trans* A and *cis* B conformers (Figure 1a). In **2**, the *cis* conformer is disordered

https://dx.doi.org/10.1021/acs.inorgchem.0c01069
Inorg. Chem. XXXX, XXX, XXX−XXX

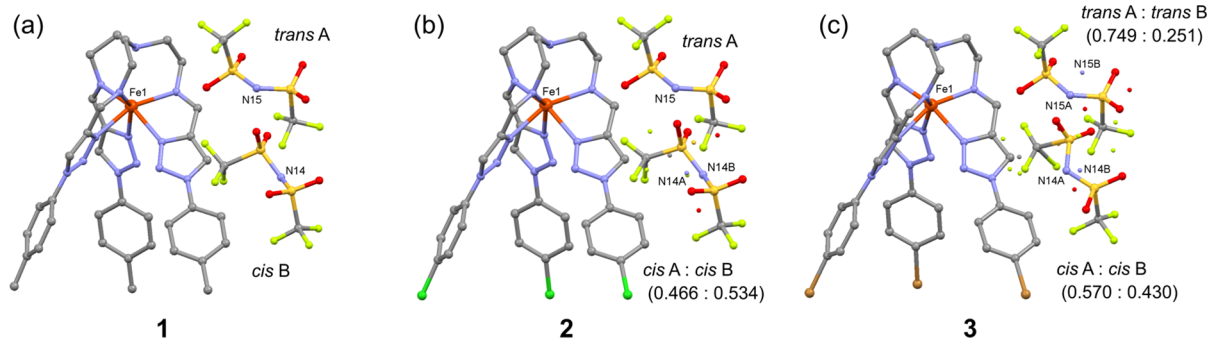

Figure 1. Molecular structures of (a) HS **1**, (b) HS **2**, and (c) HS **3** at 296 K. When the NTf_2 anions are disordered over two positions, the anion with higher occupancy is represented (atoms with lower occupancy are also indicated as small dots). Hydrogen atoms have been omitted for clarity. [Color code: Fe, orange; N, blue; C, gray; O, red; S, yellow; F, light green; Cl, green; Br, brown.]

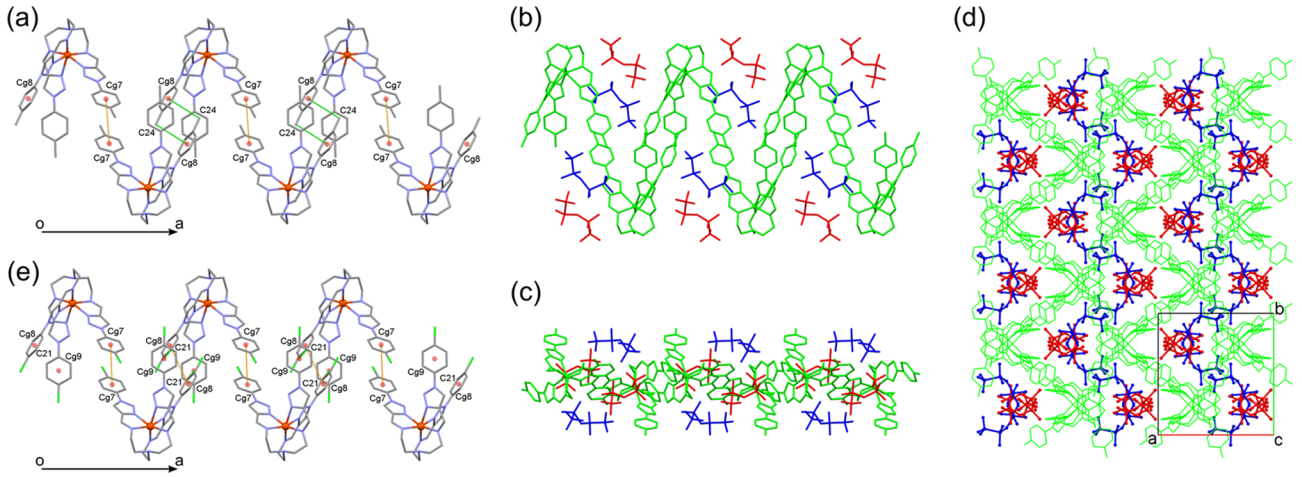

Figure 2. (a) 1D zigzag chain of complex cations of **1** at 296 K parallel to the *a*-axis constructed by intermolecular $\pi-\pi$ (Cg7···Cg7, orange dotted lines) and CH···π (C24−H26···Cg8, light green dotted lines) interactions. (b) Side view of the 1D zigzag chain of complex cations of **1** at 296 K with *cis*- and *trans*-NTf_2 anions occupying the space in the chain. (c) Top view of the 1D chain described in panel (b). (d) Crystal packing of **1** at 296 K viewed along the *ab* plane. [Color code for panels (b), (c), and (d): green, complex cation; blue, *cis*-NTf_2 anion; red, *trans*-NTf_2 anion.] (e) 1D zigzag chain of complex cations of **2** at 296 K parallel to the *a*-axis constructed mainly by two types of $\pi-\pi$ interactions (Cg7···Cg7 and Cg8···Cg8). One of the $\pi-\pi$ interaction (Cg8···Cg8) is further reinforced by additional CH···π (C21−H19···Cg9) interactions. The color code of intermolecular interactions is same as that of panel (a). Hydrogen atoms have been omitted for clarity.

with the occupancy factors of *cis* A and *cis* B being 0.466 and 0.534, respectively, while the *trans* one exists as the ordered *trans* A conformer (Figure 1b). Finally, both *cis* and *trans* conformers in **3** are disordered with *cis* A:*cis* B = 0.570:0.430 and *trans* A:*trans* B = 0.749:0.251, respectively (see Figure 1c).

Next, we examine the supramolecular structure of **1**−**3**. The data of intermolecular contacts[50] are gathered in Tables S10−S13 in the Supporting Information. At 296 K, complex cations of **1**, $[Fe^{II}L^{4\text{-Me-Ph}}]^{2+}$, are connected by intermolecular $\pi-\pi$ and CH···π interactions, forming a 1D zigzag chain parallel to the *a*-direction (see Figure 2a, as well as Tables S11 and S12). In addition, *cis*- and *trans*-NTf_2 anions occupy the space in the 1D zigzag chain (see Figures 2b and 2c). As a whole, complex cations and NTf_2 anions are connected via intermolecular CH···O hydrogen bonding interactions, constructing a 3D supramolecular network (see Figure 2d, as well as Table S13). **2** and **3** have very similar crystal packing and 3D supramolecular structure to those of **1** (see Figure S3 in the Supporting Information), whereas the 1D zigzag chain of complex cations of **2** and **3** along the *a*-axis is mainly constructed by two types of $\pi-\pi$ interactions and is further reinforced by additional CH···π interactions (see Figure 2e, as well as Figure S4 and Tables S11 and S12 in the Supporting Information). In this way, subtle change of the terminal substituents in the tripodal ligand $L^{4\text{-R-Ph}}$ (namely, R = Me, Cl, and Br) affords same coordination sphere of complex cations with the same Fe^{II} HS state, and similar packing arrangement with similar 3D supramolecular network, but drastically different ordering manner of NTf_2 anions with slightly different 1D connection of complex cations.

At 296 K, while complex **4** crystallizes in the triclinic space group $P\bar{1}$, its molecular packing is similar to that of **1**−**3** (see Figure S3). In **4**, the crystallographic unique unit consists of two distinct complex cations, $[Fe(1)L^{4\text{-MeO-Ph}}]^{2+}$ and $[Fe(2)\text{-}L^{4\text{-MeO-Ph}}]^{2+}$, and four NTf_2 anions (see Figures 3a and 3b). The $Fe-N_{ave}$ of both sites are 2.214 Å (Fe1−N) and 2.204 Å (Fe2−N), respectively, which are assignable to the Fe^{II} HS state. In addition to the $Fe-N_{ave}$, the values of Σ, Θ, S(Oh), and V_{Oh} for both Fe^{II} sites of **4** are in the similar range of those of HS **1**−**3** at 296 K, indicating that the choice of R has not impacted on the RT coordination sphere and related spin state of the present Fe^{II} family in any significant way. Aside from this, the conformation of terminal MeO groups of Fe1 site is different from that of the Fe2 site (see Figures 3a and 3b, as well as Figure S5 in the Supporting Information). In the Fe1 site, the methyl carbon of the MeO group ($H_3C12-O1$) of the

https://dx.doi.org/10.1021/acs.inorgchem.0c01069
Inorg. Chem. XXXX, XXX, XXX−XXX

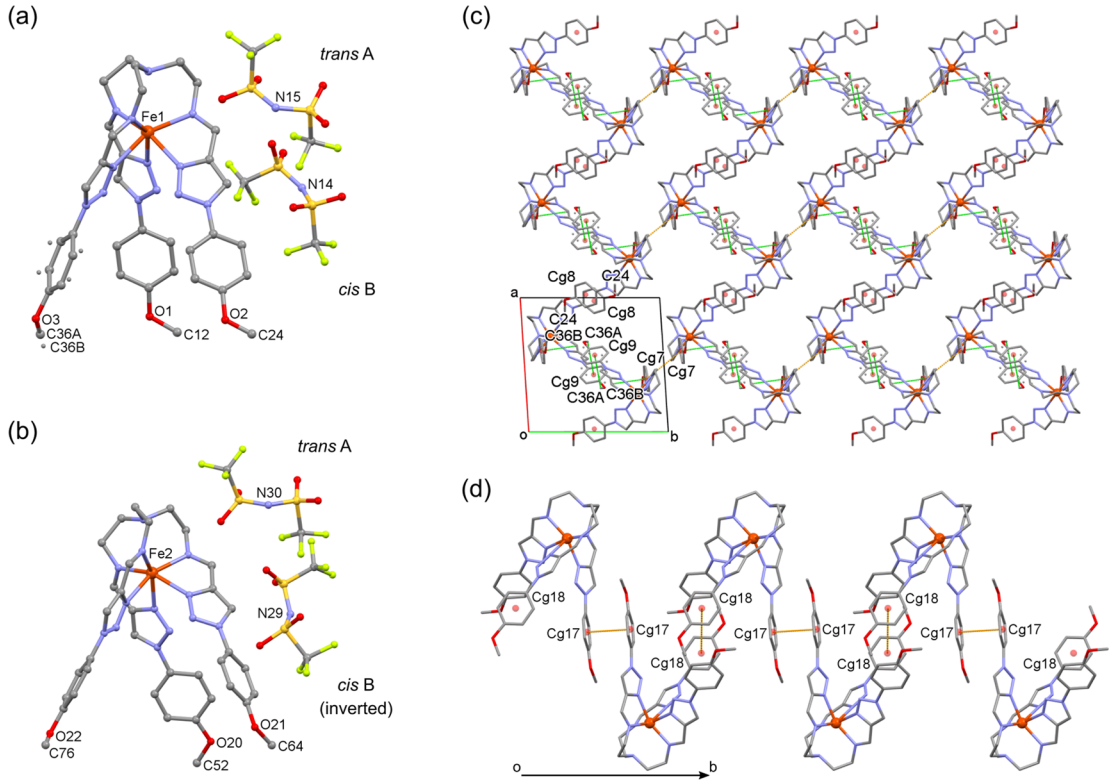

Figure 3. Molecular structures of the two distinct metal sites HS Δ-$[Fe(1)L^{4\text{-MeO-Ph}}](NTf_2)_2$ (a) and HS Δ-$[Fe(2)L^{4\text{-MeO-Ph}}](NTf_2)_2$ (b) of **4** at 296 K. (c) Molecular arrangement of Fe1 complex cations in the crystal lattice of **4** at 296 K viewed along the *ab* plane. (d) 1D zigzag chain of Fe2 complex cations of **4** at 296 K parallel to the *b*-axis constructed by two types of $\pi-\pi$ interactions. The disordered 4-MeO-Ph group with higher occupancy is represented (atoms with lower occupancy are also indicated as small dots) for panels (a) and (c). The color code of intermolecular interactions for panels (c) and (d) is the same as that of Figure 2. Hydrogen atoms have been omitted for clarity.

Δ(clockwise)−Fe1 complex cation is extended in a clockwise direction while that of the MeO group ($H_3C24-O2$) is extended in an anticlockwise direction. The last MeO group ($H_3C36-O3$) is extended in both clockwise ($H_3C36A-O3$) and anticlockwise ($H_3C36B-O3$) directions, because of the disordering of the 4-MeO-Ph group over two positions with the occupancy factors of 4-MeO-Ph A and 4-MeO-Ph B being 0.684 and 0.316, respectively. On the other hand, three methyl carbons of all MeO groups of the Δ(clockwise)-Fe2 complex cation are extended in an anticlockwise direction. It is also noteworthy that all NTf_2 anions are ordered as two crystallographically distinct *cis* B conformers and two distinct *trans* A conformers, in which one of the two *cis* B conformers locates in the lattice as an inverted molecule, compared to that of **1**−**3** (see Figures 3a and 3b). In the lattice, neighboring Fe2 cations are connected by two types of $\pi-\pi$ interactions, forming a 1D zigzag chain along the *b*-direction, whereas neighboring Fe1 cations are connected by intermolecular $\pi-\pi$ and CH···π interactions, forming a 1D zigzag chain parallel to the *b*-direction (see Figures 3c and 3d, as well as Tables S11 and S12), and are further connected through additional CH···π interactions upon cooling to form a 2D supramolecular network (vide infra). In addition, these cations and NTf_2 anions are further connected by intermolecular CH···O/F hydrogen bonding interactions, forming a 3D supramolecular network (see Figure S6 and Table S13 in the Supporting Information). As a consequence, intermolecular interactions of **4** as components of the 3D supramolecular network are comparatively different from those of **1**−**3**, while the packing arrangement is still similar to those of **1**−**3**.

Powder X-ray Diffraction (PXRD) Studies at 296 K. As shown in Figure S7 in the Supporting Information, peak positions of the experimental PXRD patterns of **1**−**4** at 296 K are in good agreement with those of the simulated patterns from the single-crystal X-ray structural data at 296 K, indicating the phase purity of the bulk crystalline samples used in the magnetic, Mössbauer spectroscopic, XAFS, and DSC studies.

Magnetic Properties. The magnetic susceptibilities of **1**−**4** were measured in the temperature range of 5−300 K, at a sweep rate of 1 K min^{-1}, in an applied magnetic field of 0.5 T. Figure 4 shows the $\chi_M T$ versus T plots of **1**−**4** in the cooling and heating modes, where χ_M is the molar magnetic susceptibility and T is the absolute temperature. The $\chi_M T$ value of **1** is constant with the value of ca. 3.3 cm^3 K mol^{-1} in the 13−300 K temperature range and decreases steeply below 12 K, indicating that **1** is a HS Fe^{II} complex ($S = 2$). Except for **1**, **2**−**4** show a variety of SCO behaviors, such as half-SCO between HS to $^1/_2$(HS + LS) for **4**, gradual two-step SCO for **3**, and three-step SCO with the combination of gradual and abrupt transition with hysteresis for **2**. The SCO behavior of each compound is detailed in turn as follows.

At 300 K, the $\chi_M T$ value of **2** is ca. 3.5 cm^3 K mol^{-1}, which is compatible with the typical value for a HS Fe^{II} species ($S = 2$). Upon cooling from 300 K, the $\chi_M T$ value continuously decreases to a value of ca. 0.1 cm^3 K mol^{-1} at 5 K, indicating the complete HS → LS spin transition. In this transition, three different steps were observed: a first gradual decrease between 300 K and 195 K, a second gradual one between 177 K and 151 K, and a third abrupt one between 143 K and 137 K. At

https://dx.doi.org/10.1021/acs.inorgchem.0c01069
Inorg. Chem. XXXX, XXX, XXX−XXX

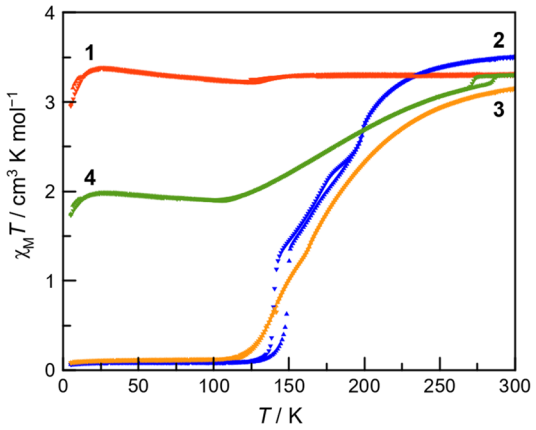

Figure 4. $\chi_M T$ vs T plots of **1** (red), **2** (blue), **3** (orange), and **4** (green) at a sweep rate of 1 K min^{-1} in the cooling (inverted triangles) and heating (triangles) modes.

the first narrow plateau with a width of ∼18 K centered at ca. 186 K, the $\chi_M T$ value is ca. 2.3 cm^3 K mol^{-1}, expected for an approximately two-thirds of Fe^{II} sites are HS state (INT1 phase). At a second narrow plateau with a width of ∼8 K centered at ca. 147 K, the $\chi_M T$ value is ca. 1.4 cm^3 K mol^{-1}, expected for approximately one-third of the Fe^{II} sites are HS state (INT2 phase). Upon heating from 5 K, a thermal hysteresis with a width of 8 K was observed during the LS ↔ INT2 transition [The critical temperatures for the cooling ($T_{1/2\downarrow}$) and heating ($T_{1/2\uparrow}$) modes (140 and 148 K, respectively).] This thermal hysteresis was also observed by the measurement in the settle mode (see Figure S8 in the Supporting Information) and was retained for at least three consecutive thermal cycles (see Figure S9a in the Supporting Information). In addition, during the INT2 → INT1 transition, a small difference compared with the initial cooling mode was observed.

For **3**, the $\chi_M T$ value is 3.1 cm^3 K mol^{-1} at 300 K, which is consistent with the theoretical value for a HS Fe^{II} species (S = 2). Upon cooling, the $\chi_M T$ value gradually decreases from a value of 3.1 cm^3 K mol^{-1} at 300 K to a plateau value of ca. 0.1 cm^3 K mol^{-1} in the temperature region of <120 K, typical of a LS state (S = 0). In this transition, two different steps were observed: a gradual decrease between 300 K and 160 K and a more abrupt one between 160 K and 112 K. The magnetic behaviors observed during cooling and heating modes are similar to each other with no hysteresis.

The $\chi_M T$ versus T plots for **4** show a gradual half-SCO with unusual hysteresis. The $\chi_M T$ value at 300 K is 3.3 cm^3 K mol^{-1}, which is compatible with the theoretical value for a HS Fe^{II} species (S = 2). Upon cooling the temperature from 300 K, the $\chi_M T$ value steeply decreases from 3.3 cm^3 K mol^{-1} at 275 K to 3.2 cm^3 K mol^{-1} at 269 K, and then gradually decreases in 269−107 K, and then reaches a plateau value of ca. 1.9 cm^3 K mol^{-1} below 104 K. This $\chi_M T$ value is approximately half of the 3.3 cm^3 K mol^{-1} at 300 K, indicating that one of two Fe^{II} sites converts to the LS state, while other remains in the HS state. Upon heating from 5 K, the magnetic behavior is similar to that observed in a cooling mode at temperatures below 269 K. Further warming causes the abrupt increase of the $\chi_M T$ value from 3.2 cm^3 K mol^{-1} at 283 K to 3.3 cm^3 K mol^{-1} at 288 K. The critical temperatures for the cooling ($T_{1/2\downarrow}$) and heating ($T_{1/2\uparrow}$) modes of unusual small $\chi_M T$ steps around 269−288 K are 273 and 285 K, respectively, indicating the occurrence of ca. 12 K thermal hysteresis, and the thermal hysteresis was reproducible over at least three successive thermal cycles (Figure S9b in the Supporting Information). This magnetic anomaly may be brought on by the slight modulation of the coordination geometry of the Fe^{II} ion and its resulting g-factor,[51−54] because of the order−disorder transition of the 4-MeO-Ph group of the ligand (vide infra). Anyway, subtle modification of the remote substituents of the tripodal ligand (namely, Me, Cl, Br, and MeO groups)

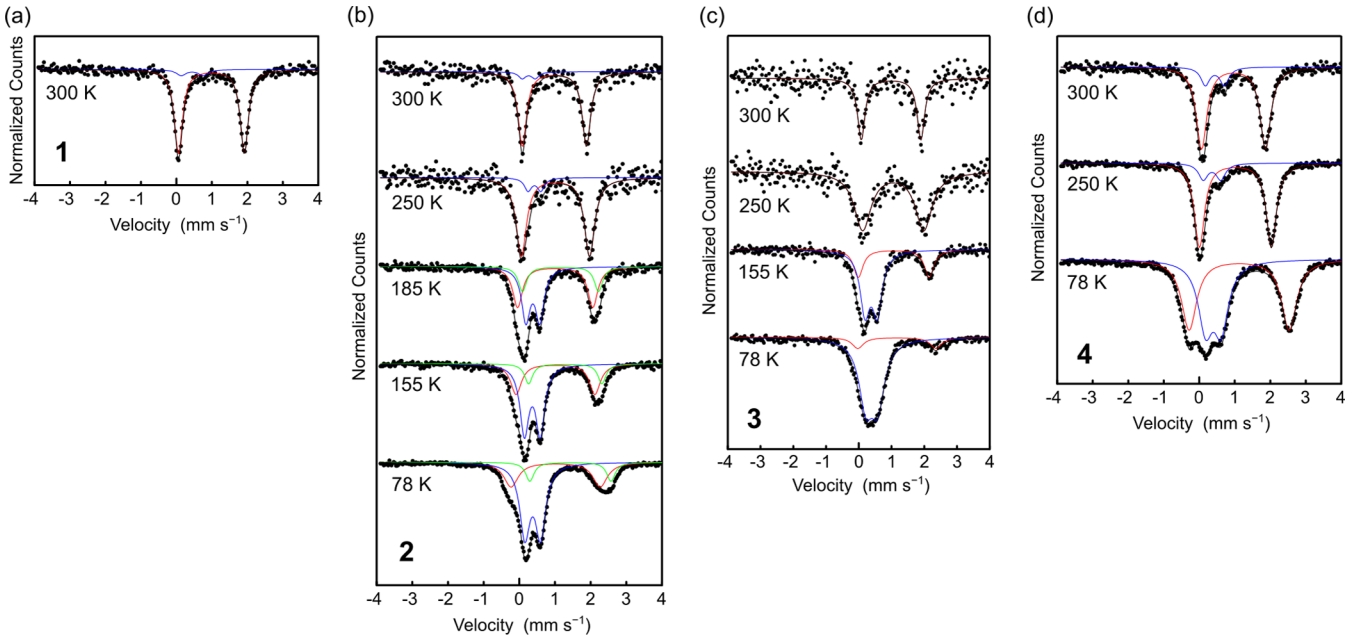

Figure 5. Variable-temperature ^{57}Fe Mössbauer spectra for (a) **1**, (b) **2**, (c) **3**, and (d) **4**. Solid lines correspond to HS (red and green) and LS (blue) sites.

https://dx.doi.org/10.1021/acs.inorgchem.0c01069
Inorg. Chem. XXXX, XXX, XXX−XXX

Table 3. Mössbauer Parameters for 1, 2, 3, and 4

Spin State		HS Fe^{II}				HS Fe^{II}				LS Fe^{II}			
complex	T, K	area, %	δ,[a] mm s^{-1}	ΔE_Q,[b] mm s^{-1}	Γ,[c] mm s^{-1}	area, %	δ,[a] mm s^{-1}	ΔE_Q,[b] mm s^{-1}	Γ,[c] mm s^{-1}	area, %	δ,[a] mm s^{-1}	ΔE_Q,[b] mm s^{-1}	Γ,[c] mm s^{-1}
1	300	92.2	0.99	1.86	0.28					7.8	0.45	0.62	0.33
2	300	93.0	0.98	1.80	0.29					7.0	0.26	0.37	0.25
	250	89.7	1.01	1.91	0.35					10.3	0.43	0.36	0.25
	185	38.1	1.01	2.11	0.33	19.6	1.16	2.13	0.28	42.3	0.38	0.39	0.29
	155	30.3	1.01	2.21	0.37	14.6	1.29	2.05	0.27	55.1	0.37	0.44	0.30
	78	28.6	1.02	2.50	0.49	12.8	1.43	2.27	0.28	58.6	0.38	0.44	0.35
3	300	100.0	0.99	1.82	0.28								
	250	100.0	1.05	1.87	0.62								
	155	31.1	1.07	2.16	0.35					68.9	0.38	0.38	0.36
	78	13.0	1.16	2.39	0.42					87.0	0.40	0.36	0.51
4	300	84.5	0.97	1.80	0.36					15.5	0.44	0.54	0.30
	250	84.9	1.02	2.03	0.34					15.1	0.36	0.49	0.32
	78	52.8	1.12	2.82	0.51					47.2	0.40	0.44	0.50

[a]Isomer shift (δ) data are reported with respect to iron foil. [b]Quadrupole splitting. [c]Full width (at the half-maximum) of the lines.

drastically affects the temperature-dependent magnetic response in this Fe^{II} family.

Mössbauer Spectroscopic Studies. Variable-temperature ^{57}Fe Mössbauer spectra for **1**−**4** were recorded in transmission mode to characterize the spin state of the Fe^{II} center (see Figure 5 and Table 3). At 300 K, the spectra of all compounds are generally dominated by a HS Fe^{II} doublet with similar isomer shift (δ) and quadrupole splitting (ΔE_Q) values, in agreement with the susceptibilities measurements. After the measurements at 300 K, **2**, **3**, and **4** were cooled to a temperature below 100 K within 50 min, then waited until the temperature was reached 78 K (ca. 30−90 min). Upon elevating the temperature after the measurements at 78 K with the rate of temperature change being 1 K min^{-1}, the doublet for HS Fe^{II} increases for **2** and **3**, indicating the occurrence of LS → HS transition (Figures 5b and 5c). Interestingly, the spectra of **2** at 185 and 155 K show two distinct HS doublets and a LS doublet, indicating that at least two Fe^{II} sites are distinguished in the INT1 and INT2 phases, respectively. However, at lowest temperature (78 K), the spectra of both **2** and **3** show the remaining HS doublets, which is inconsistent with the magnetic results in Figure 4. This inconsistency indicates the possibility of a frozen-in effect[35,36,55−58] by rapid cooling. Thus, we performed susceptibilities measurements with rapid cooling (10 K min^{-1}). Indeed, both compounds keep the larger $\chi_M T$ values below ca. 125 K than those of slower cooling rate (1 K min^{-1}; see Figure 4), indicating the occurrence of a small frozen-in effect (see Figure S10 in the Supporting Information). Furthermore, the $\chi_M T$ value of ca. 0.7 cm^3 K mol^{-1} for **2** below 125 K is larger than that of **3** (ca. 0.3 cm^3 K mol^{-1}), suggesting that **2** traps HS species more efficiently than **3** by rapid cooling. This tendency is consistent with the Mössbauer spectra at 78 K.

In **4**, the spectrum at 250 K (measured after cooling from 300 K at a rate of temperature change being 1 K min^{-1}) is similar to that of at 300 K (Figure 5d), while the $\chi_M T$ values between these temperatures have a very small step with hysteresis (vide supra). At lowest temperature (78 K), the spectrum shows the two doublets assignable to the Fe^{II} with HS:LS = 1:1. It agrees well with the magnetic results and also the crystal structure (vide infra).

XAFS Studies. Figure 6 shows the temperature-dependent XAFS spectra for **1**−**4** for Fe *K*-edge. Spectral line shapes and

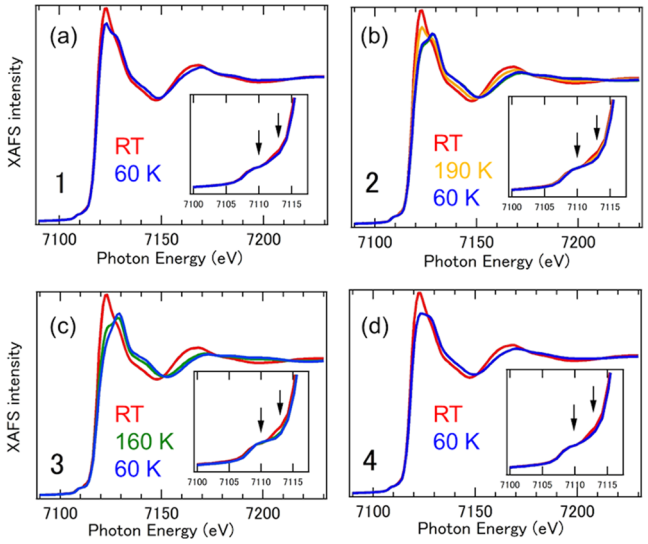

Figure 6. Temperature-dependent XAFS spectra of (a) **1**, (b) **2**, (c) **3**, and (d) **4**. Inset in each panel displays the expanded region around pre-edges. Arrows indicate the peak positions.

peak positions confirm the Fe^{II} ionic states for all complexes. Main peak in Fe *K*-edge shifts toward the higher photon energy side with decreasing temperature through SCO. These shifts are explained by the changes between HS and LS states, because of the modulation of the ligand field strength by temperature, which is derived from the small ionic radii in LS states determined by XRD (vide infra). Small but finite intensities in pre-edge structures appear at ∼7110 eV, which are originated from the transition between 1*s* and 3*d* levels through the prohibited transitions. Considering the ligand field symmetry, $^4T_{1g}$ and $^4T_{2g}$ multiplets in HS states and ^2E_g multiplet in LS states become the candidates for the pre-

https://dx.doi.org/10.1021/acs.inorgchem.0c01069
Inorg. Chem. XXXX, XXX, XXX−XXX

edge structures. The pre-edge structures consist of two types of peaks at 7110 and 7113 eV. At the HS states, higher energy sides are enhanced, which is consistent with the previous analysis.[59] In **1**, line shapes remain unchanged for RT and 60 K. In **2** and **3**, line shapes changed to those in LS states, which is consistent with Mössbauer and magnetic susceptibility measurements. These suggest that the Fe^{II} sites are strongly affected by the ligand field.

DSC Study for 4. To investigate the unusual hysteretic behavior of **4** in the temperature region of 269−288 K of magnetic study in more detail, DSC data were collected in the cooling and heating modes at a sweep rate of 5 K min^{-1} (Figure 7). As shown in Figure 7, a pair of exothermic and

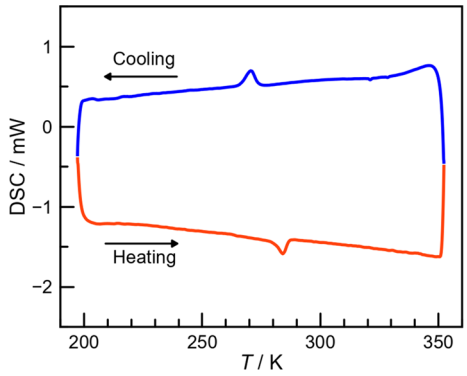

Figure 7. DSC curves of **4** recorded over the temperature range of 197−352 K in the cooling (blue) and heating (red) modes at a scan rate of 5 K min^{-1}.

endothermic peaks with $T_{max\downarrow}$= 271 K and $T_{max\uparrow}$ = 284 K is detected. The enthalpy (ΔH) and entropy (ΔS) changes are 1.5 kJ mol^{-1} and 5.5 J K^{-1} mol^{-1}, respectively, for the cooling mode, and 1.8 kJ mol^{-1} and 6.2 J K^{-1} mol^{-1}, respectively, for the heating mode. These ΔS values correspond to the value of ΔS = 5.76 J K^{-1} mol^{-1} from the Boltzmann equation, $\Delta S = R \ln N$ with N = 2 (where R is the gas constant and N represents the ratio of possible conformations).[53] This result suggests that the disordering of the 4-MeO-Ph group over two positions in the high-temperature phase from the completely ordered low-temperature phase is mainly responsible for the entropy gain (vide infra). It is also noted that these exothermic and endothermic peaks was retained for at least three consecutive thermal cycles (see Figure S11 in the Supporting Information).

Variable-Temperature X-ray Crystal Structure Analyses. Temperature-dependent X-ray diffraction data for **1**−**4** were collected to reveal the structural origin of their quite different magnetic properties. In HS compound **1**, there are no remarkable changes in the molecular level between 296, 160, and 113 K (see Figure 8a, as well as Table S5 in the Supporting Information) reflecting its spin state, while the unit cell contracts with the 4.0% volume reduction from 296 K to 113 K, arising in association with the shortening of all three axes and narrowing of the angle β (Table S1 in the Supporting Information). Upon this lattice contraction with the temperature reduction, almost all intermolecular interactions shorten (Tables S10−S13). In this situation, the nearest Fe···Fe distance along the 1D chain of complex cations [i.e., along the a-axis, hereafter abbreviated as Fe···Fe(1D)] decreases from 13.312 Å (296 K) to 13.123 Å (113 K) (see Figure S12 in the Supporting Information). Two distinct NTf_2 counteranions retain their ordered *trans* A and *cis* B conformations in these temperatures (see Table S9).

In **2**, upon lowering the temperature from 296 K to 103 K, the complex keeps the RT monoclinic space group $P2_1/c$, except for at 185 K (Table S2). The Fe−N_{ave} decreases from 2.209 Å at 296 K to 1.970 Å at 103 K, indicating the complete Fe^{II} HS to LS transition, and the temperature dependence of the Fe−N_{ave} reproduce the SCO profile (see Figure 8b and Table S6). In addition, the structural parameters Σ, Θ, S(Oh), and V_{Oh} decrease significantly from those observed at 296 K to those observed at 103 K ($\Delta\Sigma$ = 70.5°, $\Delta\Theta$ = 91.4°, ΔS(Oh) = 1.777, and ΔV_{Oh} = 3.208 $Å^3$), also indicating a rearrangement of N_6 coordination sphere to a more regular octahedral geometry upon HS → LS SCO (see Table S6). The unit cell contracts with the 3.7% volume reduction from 296 K (HS state) to 103 K (LS state). Interestingly, only the a-axis lengthens anisotropically upon this cell contraction, which is obviously different from the shortening of all axes observed in **1**. This elongation of the a-axis corresponds to the direction of the 1D zigzag chain of complex cations with the increase of Fe···Fe(1D) from 13.414 Å (296 K) to 13.641 Å (103 K) (see Figure S13 in the Supporting Information). Upon lowering the temperature, almost all intermolecular interactions shorten, and the number of CH···X hydrogen bonding interactions increases, including a few additional CH···N and CH···F contacts (see Tables S10−S13). Temperature-dependent occupancy factors of disordered *cis* and *trans* conformers of NTf_2 anions are shown in Figure 9a and Table S9. Upon lowering the temperature from 296 K to 103 K, the initially ordered *trans* A anion becomes increasingly disordered, resulting in the increase of the ratio of the *trans* B form, finally reaching the perfectly ordered *trans* B at 103 K (see Figure S14a (LS state) in the Supporting Information). On the other hand, in the initially disordered *cis* anion (*cis* A:*cis* B = 0.466:0534 at 296 K), after the initial decrease of the ratio of *cis* A between 296 K and 260 K, the ratio of *cis* A slightly increases from 260 K to 200 K to reach almost a 1:1 ratio of *cis* A and *cis* B, then decreases to reach the ratio of 0.332 (average value of three *cis* A sites, vide infra) at 185 K. This ratio is almost retained between 185 K and 163 K, and finally the *cis* anion is perfectly ordered as *cis* B conformer at 103 K (Figure S14a (LS state)).

The structural data of **2** at 185 K indicates a tripled cell with monoclinic space group $P2_1/n$. In this tripled cell, three crystallographically independent Fe^{II} sites assignable to the combination of HS site 1 (Fe1−N_{ave} = 2.191 Å), HS site 2 (Fe2−N_{ave} = 2.191 Å), and LS site (Fe3−N_{ave} = 1.978 Å) are observed (Figure 10a and Figure S15 in the Supporting Information), which results in the formation of a 1D zigzag HS−HS−LS chain parallel to the tripled c-axis (Figure S16 in the Supporting Information). This c-direction at 185 K corresponds to the a-direction at other temperatures, and the modulation of Fe···Fe(1D) is observed in this 1D HS−HS−LS chain along the c-axis (Figure S16). The stabilization of these mixed spin states may arise from the regular arrangement of NTf_2 anions having different disordering ratio along the 1D π-stacked zigzag chain of complex cations (Figure S15 and S16). In this way, the 2/3 HS (HS−HS−LS) state at the first narrow plateau centered at ca. 186 K (INT1 phase) was structurally characterized. Unfortunately, the X-ray structural data of the INT2 phase at ∼147 K could not be obtained, which may be due to its very narrow temperature range located on the

https://dx.doi.org/10.1021/acs.inorgchem.0c01069
Inorg. Chem. XXXX, XXX, XXX−XXX

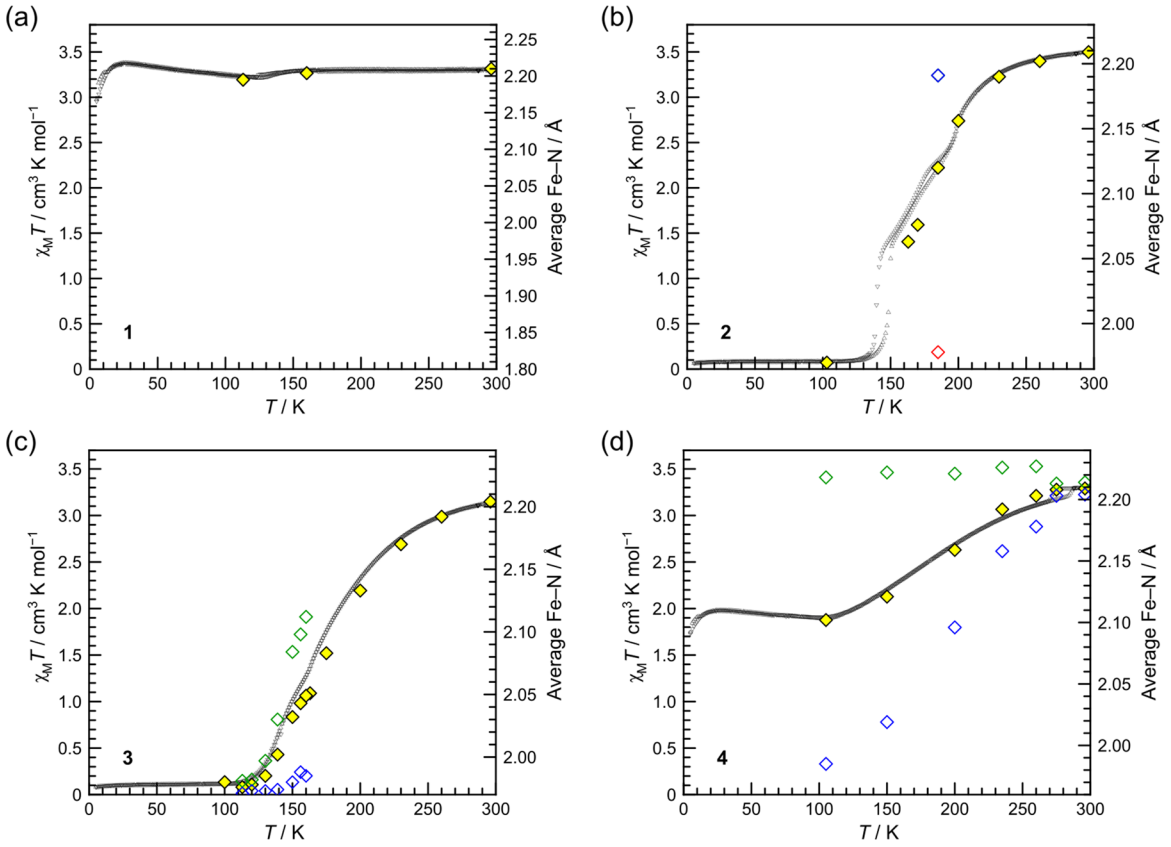

Figure 8. Temperature-dependent average Fe−N coordination bond distances (Fe−N_{ave}, yellow diamonds) with the temperature dependence of $\chi_M T$ values (black triangles) for (a) **1**, (b) **2**, (c) **3**, and (d) **4**. [Color code: Fe1 site (HS), green; Fe2 site (HS), blue; Fe3 site (LS), red for **2** at 185 K. Fe1 site, green; Fe2 site (LS), blue for **3**. Fe1 site (HS), green; Fe2 site, blue for **4**.]

boundary between a higher-temperature gradual SCO region and a lower-temperature hysteretic abrupt SCO region.

In **3**, upon lowering the temperature from 296 K to 163 K, the complex keeps the RT monoclinic space group $P2_1/c$, then changes to the doubled cell with the monoclinic space group $P2_1/n$ at 160 K (see Table S3). After that, the doubled cell is retained until 113 K, and finally **3** reaches initial monoclinic space group $P2_1/c$ at 100 K. The Fe−N_{ave} decreases from 2.204 Å at 296 K to 1.980 Å at 100 K, indicating the complete Fe^{II} HS to LS transition, and the temperature dependence of the Fe−N_{ave} reproduce the form of stepped gradual SCO (Figure 8c and Table S7). While HS **3** also shows the decreasing of Σ, Θ, S(Oh), and V_{Oh} upon HS → LS SCO from 296 K to 100 K similar to that of HS **2**, variations of these values are smaller than those of **2** (ΔΣ = 66.0°, ΔΘ = 80.2°, ΔS(Oh) = 1.636, and ΔV_{Oh} = 3.012 Å^3). In the temperature region between 160 K and 113 K (doubled cell), two crystallographically independent complex-cation sites are observed. At 160 K, the Fe2 site is LS (Fe2−N_{ave} = 1.985 Å), while the Fe1 site is a mixture of HS and LS (Fe1−N_{ave} = 2.112 Å). Upon lowering the temperature from 160 K, the Fe2 site shows no remarkable structural change, while the Fe1 site shows the shortening of Fe−N distances, finally reaches the LS state at 113 K (Fe1−N_{ave} = 1.981 Å). In this temperature region, the structure consists of stripes of Fe1 and Fe2 layers alternating in a Fe1−Fe2−Fe1−Fe2 manner (Figure 10b). The unit cell contracts with the 3.7% volume reduction from 296 K (HS state) to 100 K (LS state). As in the case with **2**, **3** shows anisotropic *a*-axis lengthening upon cooling, which is related to the expansion of the 1D zigzag chain with the slight increase of Fe···Fe(1D) from 13.648 Å (296 K) to 13.749 Å (100 K) (see Figure S17 in the Supporting Information). However, in the temperature region between 160 K and 113 K (doubled *a*-axis), the undulated two Fe···Fe(1D) distances (i.e., Fe1 → Fe2 and Fe2 → Fe1) along the 1D zigzag chain show different temperature dependencies, that is, lengthening and shortening upon cooling, respectively (see Figure S18 in the Supporting Information). Overall, in the lattice, the shortening of almost all intermolecular interactions and the increase in the number of CH···X hydrogen bonding interactions including a few additional CH···N/F contacts are occurred upon cooling (Tables S10−S13). Temperature-dependent occupancy factors of disordered *cis* and *trans* conformers of NTf_2 anions are shown in Figure 9b and Table S9. Upon lowering the temperature from 296 K to 163 K, the ratio of *trans* A gradually decreases to reach almost 1:1 of *trans* A and *trans* B at 163 K, while the ratio of *cis* A gradually increases to reach the ratio of 0.681 at 175 K, then suddenly decreases to reach almost 1:1 of *cis* A and *cis* B at 163 K. After that, all NTf_2 anions are ordered between 160 K (Figure S19 in the Supporting Information) and 113 K, in which there are two crystallographically independent *cis* conformers (*cis* A and *cis* B) and *trans* conformers (*trans* A and *trans* B). Therefore, the effect on the SCO of the anion conformation change is negligible from 160 K to 113 K, while the stabilization of mixed two Fe^{II} sites may arise from the alternate arrangement of A and B conformers of NTf_2 anions along the 1D π-stacked zigzag chain of complex cations (see Figures S18 and S19). Finally, both *cis* and *trans* anions are disordered again, with a higher ratio of B forming

https://dx.doi.org/10.1021/acs.inorgchem.0c01069
Inorg. Chem. XXXX, XXX, XXX−XXX

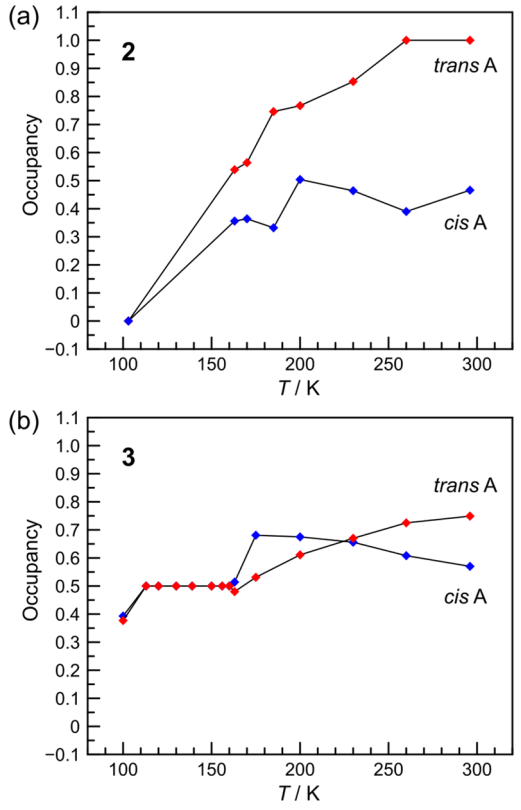

Figure 9. Temperature-dependent occupancy factors of *cis* A (blue) and *trans* A (red) conformers of NTf_2 anions for (a) **2** and (b) **3**.

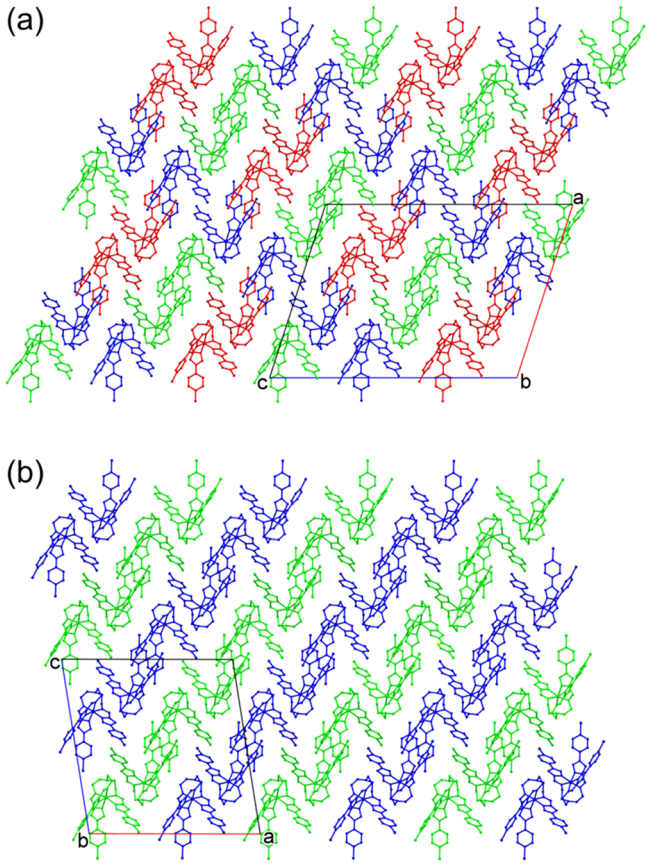

Figure 10. Packing of intermediate phases of (a) **2** at 185 K and (b) **3** at 160 K. [Color code: Fe1 site (HS), green; Fe2 site (HS), blue; Fe3 site (LS), red (for **2**); Fe1 site, green (mixture of HS and LS); Fe2 site (LS), blue (for **3**). Hydrogen atoms and NTf_2 anions have been omitted for clarity.]

than A (*cis* A:*cis* B = 0.393:0.607, and *trans* A:*trans* B = 0.377:0.623) at 100 K (Figure S14b (LS state)).

On the whole, unlike the methyl-substituted **1**, in the lattice of the halogen-substituted **2** and **3**, elastic frustration is generated by the antagonistic interactions (i.e., cation···cation and cation···anion interactions via intermolecular contacts) mainly along the 1D zigzag chain, and such elastic frustration alters by thermally induced conformational change and/or order−disorder transition of intrinsically frustrated NTf_2 anions. Furthermore, this thermal dependence of anions in the lattice is drastically affected by the subtle change of substituents (Cl or Br), resulting in different SCO profile with different degree of the stabilization of various mixed spin states between **2** and **3**.

In **4**, the initial RT triclinic space group $P\bar{1}$ is retained in the entire temperature region from 296 K to 105 K. As shown in Figure 8d, only Fe2 site shows the shortening of Fe2−N_{ave} from 2.204 Å at 296 K to 1.985 Å at 105 K, corresponding to HS → LS transition, while the Fe1 site keeps the Fe1−N_{ave} of ca. 2.22 Å, indicating its HS character. The temperature dependence of the Fe−N_{ave} (averaged value of both Fe sites) agrees well with the gradual half-SCO profile (Figure 8d and Table S8). The HS Fe2 site also shows the decreasing of Σ, Θ, S(Oh), and V_{Oh} upon HS → LS SCO from 296 K to 105 K ($\Delta\Sigma$ = 64.8°, $\Delta\Theta$ = 72.8°, ΔS(Oh) = 1.671, and ΔV_{Oh} = 2.905 Å^3), whereas the HS Fe1 site shows no remarkable difference in these values, because of the absence of SCO. The unit cell contracts with the 2.9% volume reduction from 296 K (HS−HS state) to 105 K (HS−LS state). Upon lowering the temperature, the Fe···Fe(1D) of the 1D zigzag chain of Fe2 cations along the *b*-axis decreases from 13.549 Å (HS at 296 K) to 13.180 Å (LS at 105 K) (Figure S20 in the Supporting Information). This tendency is different from that of **2** and **3**, probably because of the difference of the π−π stacking mode of the 1D zigzag chain and its direction between **4** and **2**−**3**. At the same time, additional CH···π interactions between Fe1 cations are increased, finally forming the 2D supramolecular network mentioned above (Table S12). In this situation, Fe···Fe distances in the 2D assembly increase upon cooling along the intermolecular CH···π interactions (Figure S21). In the whole lattice, the number of CH···O/F contacts between cations and anions also increases, and these contacts shorten upon cooling (Table S13).

As mentioned in the magnetic properties section (vide supra), **4** shows unusual small $\chi_M T$ changes with hysteresis ($T_{1/2\downarrow}$ and $T_{1/2\uparrow}$ = 273 and 285 K, respectively). To reveal this anomaly, crystal structures at 275 K in both cooling and heating modes were determined. Upon cooling, the structure at 275 K is almost the same as that of at 296 K (see Figures S22a, S22b, S23a, and S23b in the Supporting Information). However, further cooling to 260 K shows two remarkable conformational changes: (1) the disordered 4-MeO-Ph group at 275 K is ordered, and the methyl carbon of the MeO group (H_3C36−O3) of the Δ(clockwise)-Fe1 complex cation extended in both the clockwise (H_3C36A−O3) and anticlockwise (H_3C36B−O3) directions at 275 K changes its direction to an anticlockwise direction at 260 K (Figure S22c); and (2) one of the two *cis* B conformer changes into *cis* A form (Table S9 and Figures S23c and S23d). These conformations at 260 K

https://dx.doi.org/10.1021/acs.inorgchem.0c01069
Inorg. Chem. XXXX, XXX, XXX−XXX

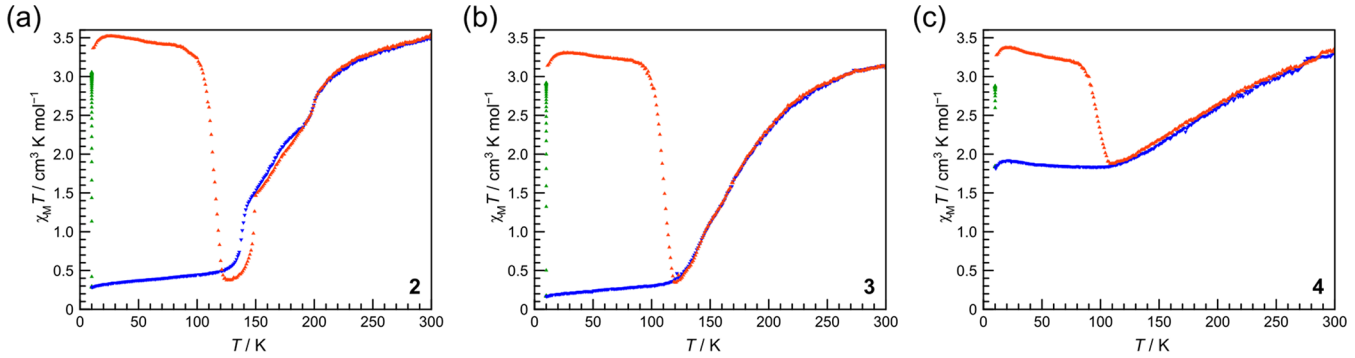

Figure 11. LIESST effect of (a) **2**, (b) **3**, and (c) **4**. Initial thermal spin transition in the cooling mode from 300 K to 10 K at a sweep rate of 2 K min^{-1}, 532 nm light irradiation at 10 K, and thermal relaxation after switching the light off are indicated as blue, green, and red triangles, respectively. The thermal relaxation process was recorded in the warming mode from 10 K at a sweep rate of 0.3 K min^{-1} until the completion of thermal relaxation (150, 130, and 130 K for **2**, **3**, and **4**, respectively) and then the temperature was increased at 2 K min^{-1} to 300 K.

are retained at lowered temperature, and interestingly, at 275 K in the heating mode (see Figures S22e, S22f, S23e, and S23f). Consequently, this conformational bistability induces hysteretic small $\chi_M T$ changes between 273 K and 285 K (see also magnetic properties and DSC study sections). Except for the above-mentioned conformational change, NTf_2 anions show no further conformational change or disordering between 296 K and 105 K. In this way, in contrast to methyl-substituted **1**, the lattice of methoxy-substituted **4** can accommodate the conformational change of the NTf_2 anion and the terminal MeO group of the ligand, allowing the partial volume change of the complex cations associated with SCO.

LIESST Experiments. Photomagnetic studies were also performed for **2**−**4**, since they showed a variety of SCO behaviors. As shown in Figure 11, as well as Figure S24 in the Supporting Information, after initial cooling from 300 K to 10 K at a sweep rate of 2 K min^{-1} in darkness, green laser light irradiation (532 nm, the power of the light is ca. 5 mW cm^{-2}) to the polycrystalline samples at 10 K for 15−20 min affords an increase of the $\chi_M T$ values with the saturated values of ca. 3.0, 2.9, and 2.9 cm^3 K mol^{-1} for **2**, **3**, and **4**, respectively, indicating efficient and almost quantitative conversion of the Fe^{II} site from the LS (for **2** and **3**) or 1/2(HS + LS) (for **4**) to the photoinduced metastable HS state. After the light was switched off, the thermal relaxation was studied. Upon elevating the temperature, the $\chi_M T$ values increase to reach the maximum values of ca. 3.5, 3.3, and 3.4 cm^3 K mol^{-1} for **2**, **3**, and **4**, respectively, and then slightly decrease. The increase of the $\chi_M T$ values from 10 K to ca. 25 K can be attributed to the zero-field splitting of the trapped Fe^{II} HS molecules (S = 2).[60] Finally, the $\chi_M T$ values decrease abruptly in a single-step manner at ∼95−120 K (for **2** and **3**), and at ∼85−105 K (for **4**) to reach the thermally stable LS state (for **2** and **3**), and 1/2(HS + LS) state (for **4**). The T(LIESST) values[61] determined from the $d\chi_M T/dT$ vs T curve in the warming mode at a sweep rate of 0.3 K min^{-1} are 113, 111, and 97 K for **2**, **3**, and **4**, respectively.

Létard et al. have reported the linear correlation between T(LIESST) and $T_{1/2}$ values with the general equation $T(\text{LIESST}) = T_0 - 0.3T_{1/2}$, which was constructed by the comprehensive examination of a large number of SCO compounds.[61] To reveal the T_0 value of the present ligand system, first, the $T_{1/2}$ values of **2**−**4** were estimated. Since **2**−**4** have a variety of thermal SCO profiles including the combination of stepwise, gradual, abrupt, and hysteretic natures, the temperature of the middle point (HS:LS = 50:50) of the overall SCO between complete HS and LS states for **2** and **3** or the middle point of the complete HS−HS and HS−LS states for **4** was used as the $T_{1/2}$ value. The estimated $T_{1/2}$ values are 165, 171, and 189 K for **2**, **3**, and **4**, respectively, resulting the estimated T_0 value of 160 K for the present triazole-containing tripodal hexadentate ligand system. It is noteworthy that the T_0 value of 160 K for **2**−**4** is much higher than that of the related complexes bearing similar imidazole-containing N_6 tripodal ligand (T_0 = 100 K).[55,56]

DFT Studies. DFT calculations for **1**−**4** were performed.[62] Based on the results of calculations with TPSSh, M06L, and B3LYP functionals (see the Supporting Information), and DFT studies reported by Cirera and co-workers,[63] we chose TPSSh functional in the present discussion.

First, we performed single-point DFT energy calculations on experimental crystal structures (Table S14 in the Supporting Information). The HS−LS energy differences (ΔE_{HS-LS}) for **1**−**4** at 296 K (−9700, −9715, −9542, −9716, and −9460 cm^{-1} for **1**, **2**, **3**, Fe1 site of **4**, and Fe2 site of **4**, respectively) reveal that the HS states are more stable in all complexes at RT. On the other hand, at 100−105 K, ΔE_{HS-LS} values are 12 783, 11 471, and 10 644 cm^{-1} for **2**, **3**, and Fe2 site of **4**, respectively, suggesting that the LS states are more stable, except for the value of −10 058 cm^{-1} for Fe1 site of **4** (the HS state is more stable). At 185 K for **2**, ΔE_{HS-LS} values are −9135, −9123, and 11 769 cm^{-1} for Fe1, Fe2, and Fe3 site, respectively, indicating that the HS state is more stable in Fe1 and Fe2 sites, whereas the LS state is more stable in Fe3 site. Finally, at 160 K for **3**, ΔE_{HS-LS} value of 10 821 cm^{-1} for Fe2 site reveals that the LS state is more stable, while the value of −4282 cm^{-1} for Fe1 site, reflecting the existence of both HS and LS species. These results are consistent with the magnetic properties and single-crystal X-ray structure analyses.

Next, we performed DFT geometry optimization calculation in the gas phase on **1**−**4** at both LS and HS states using experimental crystal structures as initial geometry. The geometrical parameters are summarized in Table S15 in the Supporting Information, and the optimized structures are shown in Figure S25 in the Supporting Information. Optimized structural parameters for **1**−**4** are similar to each other, irrespective of the remote substituents Me, Cl, Br, and MeO, and are in agreement with experimental crystal structures in each spin states. In addition, the ΔE_{HS-LS} values of these DFT optimized structures are also similar to each other (Table S19

https://dx.doi.org/10.1021/acs.inorgchem.0c01069
Inorg. Chem. XXXX, XXX, XXX−XXX

in the Supporting Information). These results indicate that the effect of the terminal substituent modification on the ligand field strength is negligible in the present Fe^{II} family. As a consequence, a variety of spin behaviors in **2**−**4** (and SCO deactivation of **1**) are surely and dominantly triggered by temperature-dependent flexible anion ordering through supramolecular network in the crystal lattice (vide supra).

CONCLUSIONS

In summary, we present here a new family of Fe^{II} complexes $[FeL^{4\text{-R-Ph}}](NTf_2)_2$, in which the subtle modification of terminal para-substituents of complex cations (i.e., R = Me, Cl, Br, and MeO for **1**, **2**, **3**, and **4**, respectively) produces remarkably distinct magnetic response, spanning temperature invariant HS state, half-, two-, and three-stepped SCO behaviors for **1**, **4**, **3**, and **2**, respectively. The three-step SCO of **2** also includes thermal hysteresis in the LS ↔ INT2 transition. Despite such different thermal SCO profiles, **2**−**4** show similar quantitative LIESST effect by green laser light irradiation at 10 K with moderately high T(LIESST) value. The electronic effect of the different substituents on magnetic properties was negligible due to the equivalence of the ligand field strength of **1**−**4** revealed by DFT calculations.

Surprisingly, the packing arrangement of the present complexes is similar to each other and generally constructed by 3D supramolecular network via intermolecular $\pi-\pi$ and CH···π interactions between complex cations, and CH···X (X = O, N, and F) hydrogen bonding interactions between complex cations and intrinsically frustrated NTf_2 anions. Comparison of the RT crystal lattice of HS **1**−**4** indicates that the existence of both perfectly ordered *cis*- and *trans*-NTf_2 anions inhibits SCO to the LS state upon cooling. **1** corresponds such no SCO system and all NTf_2 anions of **1** show no conformational change or order−disorder transition upon cooling. Although all NTf_2 anions of **4** are also ordered, one of the two distinct *cis*-conformers shows temperature-dependent conformational change. In addition, another *cis*-conformer is located in the lattice of **4** as an inverted molecule compared to that of **1**−**3**. These variable features of the NTf_2 anion are brought by the introduction of conformationally changeable MeO substituents instead of Me groups into the ligand, resulting the occurrence of half-SCO in **4**, in which the partial volume change of the complex cations associated with SCO is allowed.

On the other hand, very flexible temperature-dependent conformational change and order−disorder transition of NTf_2 anions are observed in the lattice of halogen-substituted **2** and **3**, while **1**−**3** are isomorphous. This flexible nature of the NTf_2 anions in the crystal lattice is an essential role for exhibiting complete thermal LS ↔ HS SCO in the present Fe^{II} family. In particular, temperature dependencies of occupancy factors of NTf_2 anions for **2** are very different from those of **3**, inducing different stepwise SCO behaviors, namely, two-step SCO for **3** and three-step SCO for **2**. The gentle order−disorder transition including all different NTf_2 conformers (*cis* A and B and *trans* A and B) at ∼160 K generates two-step SCO associated with the structural phase transition in **3**. Finally, in **2**, the HS, INT1, and LS phases of three-step SCO were structurally characterized by single-crystal X-ray structure analyses. A long-range ordering with 3-fold periodicity was observed in the INT 1 phase in which three Fe^{II} sites were assignable to HS1, HS2, and LS1 sites, corresponding to magnetic, Mössbauer, and XAFS data. Mössbauer spectrum at 155 K indicated that the existence of at least two distinct Fe^{II} sites in the INT2 phase which are not observed in crystal structures at 163 and 103 K. These results suggest that two different structural phase transitions are related to the occurrence of three-step SCO of **2**. With this in mind, variable-temperature X-ray structure analyses revealed that both structural phase transitions are associated with the order−disorder transition of NTf_2 anions. In particular, the order−disorder transition of both *cis* and *trans* anions between two conformers (i.e., A and B) and only one ordered conformer B is essential for exhibiting the abrupt SCO with hysteresis of the LS ↔ INT2 transition.

It is importantly noted that such flexible anion ordering propagates through the 3D supramolecular network that has the strong 1D character of directly contacted complex cations, including the NTf_2 anions in the space of the 1D zigzag chain. Therefore, the degree of elastic frustration mainly along this 1D chain is altered by thermally induced conformational change and/or order−disorder transition of intrinsically frustrated NTf_2 anions, leading to the occurrence of stepped SCO. In addition, this temperature dependence of anions and associated stepwise manner of spin transition are strongly affected by the subtle modification of remote-substituents R of the present complex cation $[FeL^{4\text{-R-Ph}}]^{2+}$.

As a whole, this study highlights that systematic control of magnetic response from no SCO to half-SCO, two-step SCO, and three-step SCO with hysteresis is successfully achieved through precise tuning of ordering of flexible NTf_2 counteranions included in the supramolecular network with potentially SCO-active complex cations by solely subtle modification of terminal para-substituents of the ligand. The findings of this work are applicable to a vast amount of known systems consisting of SCO-active complex cations and conventional counteranions, and will drive the growth of multistep hysteretic SCO materials.

ASSOCIATED CONTENT

Supporting Information

The Supporting Information is available free of charge at https://pubs.acs.org/doi/10.1021/acs.inorgchem.0c01069.

Experimental information, TG/DTA curves, IR spectra, PXRD patterns, additional $\chi_M T$ versus T and $\chi_M T$ versus time plots and DSC curves, all crystallographic data, list of all coordination bond lengths, angles, structural parameters, occupancy factors of anions, distances of intermolecular contacts, crystal structures, and the results of DFT calculations (PDF)

Cartesian coordinates of the DFT optimized geometry of **1**−**4** (ZIP)

Accession Codes

CCDC 1987703−1987735 contain the supplementary crystallographic data for this paper. These data can be obtained free of charge via www.ccdc.cam.ac.uk/data_request/cif, or by emailing data_request@ccdc.cam.ac.uk, or by contacting The Cambridge Crystallographic Data Centre, 12 Union Road, Cambridge CB2 1EZ, UK; fax: + 44 1223 336033.

AUTHOR INFORMATION

Corresponding Author

Hiroaki Hagiwara − *Department of Chemistry, Faculty of Education, Gifu University, Gifu 501-1193, Japan;*

https://dx.doi.org/10.1021/acs.inorgchem.0c01069
Inorg. Chem. XXXX, XXX, XXX−XXX

orcid.org/0000-0003-0396-7965; Email: hagiwara@gifu-u.ac.jp

Authors

Ryo Minoura − *Department of Chemistry, Faculty of Education, Gifu University, Gifu 501-1193, Japan*

Taro Udagawa − *Department of Chemistry and Biomolecular Science, Faculty of Engineering, Gifu University, Gifu 501-1193, Japan;* orcid.org/0000-0002-4072-253X

Ko Mibu − *Graduate School of Engineering, Nagoya Institute of Technology, Nagoya, Aichi 466-8555, Japan;* orcid.org/0000-0002-6416-1028

Jun Okabayashi − *Research Center for Spectrochemistry, The University of Tokyo, Bunkyo-ku, Tokyo 113-0033, Japan;* orcid.org/0000-0002-9025-2783

Complete contact information is available at: https://pubs.acs.org/10.1021/acs.inorgchem.0c01069

Notes

The authors declare no competing financial interest.

■ ACKNOWLEDGMENTS

We thank Prof. N. Kojima (The University of Tokyo, Japan) for helpful discussions, Prof. O. Sakurada (Gifu University, Japan) for assistance collecting PXRD data, and T. Onoue for Mössbauer spectroscopic measurements. This work was supported in part by JSPS KAKENHI (Grant Nos. JP18K14240 (to H.H.) and JP18K05028 (to T.U.)). A part of this work was conducted in Institute for Molecular Science (IMS), Okazaki, Japan, and Nagoya Institute of Technology (NIT), Nagoya, Japan, supported by Nanotechnology Platform Program (Molecule and Material Synthesis) of the Ministry of Education, Culture, Sports, Science and Technology (MEXT), Japan. Parts of the synchrotron radiation experiments were performed under the approval of the Photon Factory Program Advisory Committee, KEK (No. 2019G029). Portion of these computations was performed at Research Center for Computational Science (RCCS), Okazaki.

■ REFERENCES

(1) Gütlich, P.; Goodwin, H. A. Spin Crossover—An Overall Perspective. *Top. Curr. Chem.* **2004**, *233*, 1−47.

(2) Gütlich, P.; Gaspar, A. B.; Garcia, Y. Spin State Switching in Iron Coordination Compounds. *Beilstein J. Org. Chem.* **2013**, *9*, 342−391.

(3) Halcrow, M. A. *Spin-Crossover Materials: Properties and Applications*; John Wiley & Sons, 2013.

(4) Feltham, H. L. C.; Barltrop, A. S.; Brooker, S. Spin Crossover in Iron(II) Complexes of 3,4,5-Tri-Substituted-1,2,4-Triazole (Rdpt), 3,5-Di-Substituted-1,2,4-Triazolate (dpt^-), and Related Ligands. *Coord. Chem. Rev.* **2017**, *344*, 26−53.

(5) Senthil Kumar, K.; Bayeh, Y.; Gebretsadik, T.; Elemo, F.; Gebrezgiabher, M.; Thomas, M.; Ruben, M. Spin-Crossover in Iron(II)-Schiff Base Complexes. *Dalton Trans.* **2019**, *48*, 15321−15337.

(6) Kahn, O.; Martinez, C. J. Spin-Transition Polymers: From Molecular Materials toward Memory Devices. *Science* **1998**, *279* (5347), 44−48.

(7) Roubeau, O. Triazole-Based One-Dimensional Spin-Crossover Coordination Polymers. *Chem. - Eur. J.* **2012**, *18* (48), 15230−15244.

(8) Weber, B.; Bauer, W.; Obel, J. An Iron(II) Spin-Crossover Complex with a 70 K Wide Thermal Hysteresis Loop. *Angew. Chem., Int. Ed.* **2008**, *47* (52), 10098−10101.

(9) Weber, B.; Bauer, W.; Pfaffeneder, T.; Dîrtu, M. M.; Naik, A. D.; Rotaru, A.; Garcia, Y. Influence of Hydrogen Bonding on the Hysteresis Width in Iron(II) Spin-Crossover Complexes. *Eur. J. Inorg. Chem.* **2011**, *2011* (21), 3193−3206.

(10) Hayami, S.; Gu, Z. Z.; Yoshiki, H.; Fujishima, A.; Sato, O. Iron(III) Spin-Crossover Compounds with a Wide Apparent Thermal Hysteresis around Room Temperature. *J. Am. Chem. Soc.* **2001**, *123* (47), 11644−11650.

(11) Halcrow, M. A. Spin-Crossover Compounds with Wide Thermal Hysteresis. *Chem. Lett.* **2014**, *43* (8), 1178−1188.

(12) Brooker, S. Spin Crossover with Thermal Hysteresis: Practicalities and Lessons Learnt. *Chem. Soc. Rev.* **2015**, *44* (10), 2880−2892.

(13) Paez-Espejo, M.; Sy, M.; Boukheddaden, K. Elastic Frustration Causing Two-Step and Multistep Transitions in Spin-Crossover Solids: Emergence of Complex Antiferroelastic Structures. *J. Am. Chem. Soc.* **2016**, *138* (9), 3202−3210.

(14) Taniguchi, D.; Okabayashi, J.; Hotta, C. Pressure-Induced Two-Step Spin Crossover in a Double-Layered Elastic Model. *Phys. Rev. B: Condens. Matter Mater. Phys.* **2017**, *96* (17), 174104.

(15) Traiche, R.; Sy, M.; Boukheddaden, K. Elastic Frustration in 1D Spin-Crossover Chains: Evidence of Multi-Step Transitions and Self-Organizations of the Spin States. *J. Phys. Chem. C* **2018**, *122* (7), 4083−4096.

(16) Murphy, M. J.; Zenere, K. A.; Ragon, F.; Southon, P. D.; Kepert, C. J.; Neville, S. M. Guest Programmable Multistep Spin Crossover in a Porous 2-D Hofmann-Type Material. *J. Am. Chem. Soc.* **2017**, *139* (3), 1330−1335.

(17) Sciortino, N. F.; Ragon, F.; Klein, Y. M.; Housecroft, C. E.; Davies, C. G.; Jameson, G. N. L.; Chastanet, G.; Neville, S. M. Guest-Responsive Elastic Frustration "On-Off" Switching in Flexible, Two-Dimensional Spin Crossover Frameworks. *Inorg. Chem.* **2018**, *57* (17), 11068−11076.

(18) Trzop, E.; Zhang, D.; Piñeiro-Lopez, L.; Valverde-Muñoz, F. J.; Carmen Muñoz, M.; Palatinus, L.; Guerin, L.; Cailleau, H.; Real, J. A.; Collet, E. First Step Towards a Devil's Staircase in Spin-Crossover Materials. *Angew. Chem., Int. Ed.* **2016**, *55* (30), 8675−8679.

(19) Zhang, D.; Trzop, E.; Valverde-Muñoz, F. J.; Piñeiro-López, L.; Muñoz, M. C.; Collet, E.; Real, J. A. Competing Phases Involving Spin-State and Ligand Structural Orderings in a Multistable Two-Dimensional Spin Crossover Coordination Polymer. *Cryst. Growth Des.* **2017**, *17* (5), 2736−2745.

(20) Sciortino, N. F.; Zenere, K. A.; Corrigan, M. E.; Halder, G. J.; Chastanet, G.; Létard, J.-F.; Kepert, C. J.; Neville, S. M. Four-Step Iron(II) Spin State Cascade Driven by Antagonistic Solid State Interactions. *Chem. Sci.* **2017**, *8* (1), 701−707.

(21) Clements, J. E.; Price, J. R.; Neville, S. M.; Kepert, C. J. Hysteretic Four-Step Spin Crossover within a Three-Dimensional Porous Hofmann-like Material. *Angew. Chem., Int. Ed.* **2016**, *55* (48), 15105−15109.

(22) Liu, W.; Peng, Y.-Y.; Wu, S.-G.; Chen, Y.-C.; Hoque, M. N.; Ni, Z.-P.; Chen, X.-M.; Tong, M.-L. Guest-Switchable Multi-Step Spin Transitions in an Amine-Functionalized Metal-Organic Framework. *Angew. Chem., Int. Ed.* **2017**, *56* (47), 14982−14986.

(23) Zhang, C.-J.; Lian, K.-T.; Huang, G.-Z.; Bala, S.; Ni, Z.-P.; Tong, M.-L. Hysteretic Four-Step Spin-Crossover in a 3D Hofmann-Type Metal-Organic Framework with Aromatic Guest. *Chem. Commun.* **2019**, *55* (74), 11033−11036.

(24) Bousseksou, A.; Molnár, G.; Real, J. A.; Tanaka, K. Spin Crossover and Photomagnetism in Dinuclear Iron(II) Compounds. *Coord. Chem. Rev.* **2007**, *251* (13−14), 1822−1833.

(25) Murray, K. S. Advances in Polynuclear Iron(II), Iron(III) and Cobalt(II) Spin-Crossover Compounds. *Eur. J. Inorg. Chem.* **2008**, *2008* (20), 3101−3121.

(26) Hogue, R. W.; Singh, S.; Brooker, S. Spin Crossover in Discrete Polynuclear Iron(II) Complexes. *Chem. Soc. Rev.* **2018**, *47* (19), 7303−7338.

(27) Matsumoto, T.; Newton, G. N.; Shiga, T.; Hayami, S.; Matsui, Y.; Okamoto, H.; Kumai, R.; Murakami, Y.; Oshio, H. Programmable Spin-State Switching in a Mixed-Valence Spin-Crossover Iron Grid. *Nat. Commun.* **2014**, *5* (1), 3865.

(28) Hostettler, M.; Törnroos, K. W.; Chernyshov, D.; Vangdal, B.; Bürgi, H.-B. Challenges in Engineering Spin Crossover: Structures and Magnetic Properties of Six Alcohol Solvates of Iron(II) Tris(2-Picolylamine) Dichloride. *Angew. Chem., Int. Ed.* **2004**, *43* (35), 4589−4594.
(29) Wei, R.-J.; Tao, J.; Huang, R.-B.; Zheng, L.-S. Reversible and Irreversible Vapor-Induced Guest Molecule Exchange in Spin-Crossover Compounds. *Inorg. Chem.* **2011**, *50* (17), 8553−8564.
(30) Phonsri, W.; Harding, P.; Liu, L.; Telfer, S. G.; Murray, K. S.; Moubaraki, B.; Ross, T. M.; Jameson, G. N. L.; Harding, D. J. Solvent Modified Spin Crossover in an Iron(III) Complex: Phase Changes and an Exceptionally Wide Hysteresis. *Chem. Sci.* **2017**, *8* (5), 3949−3959.
(31) Phonsri, W.; Davies, C. G.; Jameson, G. N. L.; Moubaraki, B.; Ward, J. S.; Kruger, P. E.; Chastanet, G.; Murray, K. S. Symmetry Breaking above Room Temperature in an Fe(II) Spin Crossover Complex with an N_4O_2 Donor Set. *Chem. Commun.* **2017**, *53* (8), 1374−1377.
(32) Phonsri, W.; Macedo, D. S.; Vignesh, K. R.; Rajaraman, G.; Davies, C. G.; Jameson, G. N. L.; Moubaraki, B.; Ward, J. S.; Kruger, P. E.; Chastanet, G.; Murray, K. S. Halogen Substitution Effects on N_2O Schiff Base Ligands in Unprecedented Abrupt Fe^{II} Spin Crossover Complexes. *Chem. - Eur. J.* **2017**, *23* (29), 7052−7065.
(33) Nishi, K.; Matsumoto, N.; Iijima, S.; Halcrow, M. A.; Sunatsuki, Y.; Kojima, M. A Hydrogen Bond Motif Giving a Variety of Supramolecular Assembly Structures and Spin-Crossover Behaviors. *Inorg. Chem.* **2011**, *50* (22), 11303−11305.
(34) Nishi, K.; Kondo, H.; Fujinami, T.; Matsumoto, N.; Iijima, S.; Halcrow, M. A.; Sunatsuki, Y.; Kojima, M. Stepwise Spin Transition and Hysteresis of a Tetrameric Iron(II) Complex, *fac*-[Tris(2-methylimidazol-4-ylmethylidene-*n*-hexylamine)]iron(II) Chloride Hexafluorophosphate, Assembled by Imidazole···Chloride Hydrogen Bonds. *Eur. J. Inorg. Chem.* **2013**, *2013* (5-6), 927−933.
(35) Yamada, M.; Hagiwara, H.; Torigoe, H.; Matsumoto, N.; Kojima, M.; Dahan, F.; Tuchagues, J.-P.; Re, N.; Iijima, S. A Variety of Spin-Crossover Behaviors Depending on the Counter Anion: Two-Dimensional Complexes Constructed by NH···Cl^- Hydrogen Bonds, $[Fe^{II}H_3L^{Me}]Cl{\cdot}X$ (X = PF_6^-, AsF_6^-, SbF_6^-, $CF_3SO_3^-$; H_3L^{Me} = Tris[2-{[(2-methylimidazol-4-yl)methylidene]amino}ethyl]amine. *Chem. - Eur. J.* **2006**, *12* (17), 4536−4549.
(36) Sato, T.; Nishi, K.; Iijima, S.; Kojima, M.; Matsumoto, N. One-Step and Two-Step Spin-Crossover Iron(II) Complexes of ((2-Methylimidazol-4-yl)methylidene)histamine. *Inorg. Chem.* **2009**, *48* (15), 7211−7229.
(37) Nihei, M.; Tahira, H.; Takahashi, N.; Otake, Y.; Yamamura, Y.; Saito, K.; Oshio, H. Multiple Bistability and Tristability with Dual Spin-State Conversions in $[Fe(dpp)_2][Ni(mnt)_2]_2{\cdot}MeNO_2$. *J. Am. Chem. Soc.* **2010**, *132* (10), 3553−3560.
(38) Okuhata, M.; Funasako, Y.; Takahashi, K.; Mochida, T. A Spin-Crossover Ionic Liquid from the Cationic Iron(III) Schiff Base Complex. *Chem. Commun.* **2013**, *49* (69), 7662−7664.
(39) Hagiwara, H.; Minoura, R.; Okada, S.; Sunatsuki, Y. Synthesis, Structure, and Magnetic Property of a New Mononuclear Iron(II) Spin Crossover Complex with a Tripodal Ligand Containing Three 1,2,3-Triazole Groups. *Chem. Lett.* **2014**, *43* (6), 950−952.
(40) Fitzpatrick, A. J.; Trzop, E.; Müller-Bunz, H.; Dîrtu, M. M.; Garcia, Y.; Collet, E.; Morgan, G. G. Electronic vs. Structural Ordering in a Manganese(III) Spin Crossover Complex. *Chem. Commun.* **2015**, *51* (99), 17540−17543.
(41) Phukkaphan, N.; Cruickshank, D. L.; Murray, K. S.; Phonsri, W.; Harding, P.; Harding, D. J. Hysteretic Spin Crossover Driven by Anion Conformational Change. *Chem. Commun.* **2017**, *53* (70), 9801−9804.
(42) Gütlich, P.; Hauser, A.; Spiering, H. Thermal and Optical Switching of Iron(II) Complexes. *Angew. Chem., Int. Ed. Engl.* **1994**, *33* (20), 2024−2054.
(43) Dai, Z.-C.; Chen, Y.-F.; Zhang, M.; Li, S.-K.; Yang, T.-T.; Shen, L.; Wang, J.-X.; Qian, S.-S.; Zhu, H.-L.; Ye, Y.-H. Synthesis and Antifungal Activity of 1,2,3-Triazole Phenylhydrazone Derivatives. *Org. Biomol. Chem.* **2015**, *13* (2), 477−486.
(44) Hagiwara, H.; Masuda, T.; Ohno, T.; Suzuki, M.; Udagawa, T.; Murai, K. Neutral Molecular Iron(II) Complexes Showing Tunable Bistability at Above, Below, and Just Room Temperature by a Crystal Engineering Approach: Ligand Mobility into a Three-Dimensional Flexible Supramolecular Network. *Cryst. Growth Des.* **2017**, *17* (11), 6006−6019.
(45) Fatiadi, A. J. Active Manganese Dioxide Oxidation in Organic Chemistry — Part I. *Synthesis* **1976**, *1976* (2), 65−104.
(46) Nakamoto, K. *Infrared and Raman Spectra of Inorganic and Coordination Compounds, Part B: Applications in Coordination, Organometallic, and Bioinorganic Chemistry*, Sixth Edition; John Wiley & Sons, Ltd.: Hoboken, NJ, 2009.
(47) Guionneau, P.; Marchivie, M.; Bravic, G.; Létard, J.-F.; Chasseau, D. Structural Aspects of Spin Crossover. Examples of the $[Fe^{II}Ln(NCS)_2]$ Complexes. *Top. Curr. Chem.* **2004**, *234*, 97−128.
(48) Marchivie, M.; Guionneau, P.; Létard, J.-F.; Chasseau, D. Photo-Induced Spin-Transition: The Role of the Iron(II) Environment Distortion. *Acta Crystallogr., Sect. B: Struct. Sci.* **2005**, *61* (1), 25−28.
(49) Llunell, M.; Casanova, D.; Cirera, J.; Alemany, P.; Alvarez, S. *SHAPE2.1. Program for Calculating Continuous Shape Measures of Polyhedral Structures*; Universitat de Barcelona: Barcelona, Spain, 2013.
(50) Spek, A. L. Single-Crystal Structure Validation with the Program PLATON. *J. Appl. Crystallogr.* **2003**, *36* (1), 7−13.
(51) Rosario-Amorin, D.; Dechambenoit, P.; Bentaleb, A.; Rouzières, M.; Mathonière, C.; Clérac, R. Multistability at Room Temperature in a Bent-Shaped Spin-Crossover Complex Decorated with Long Alkyl Chains. *J. Am. Chem. Soc.* **2018**, *140* (1), 98−101.
(52) Valverde-Muñoz, F. J.; Seredyuk, M.; Meneses-Sánchez, M.; Muñoz, M. C.; Bartual-Murgui, C.; Real, J. A. Discrimination between Two Memory Channels by Molecular Alloying in a Doubly Bistable Spin Crossover Material. *Chem. Sci.* **2019**, *10* (13), 3807−3816.
(53) Su, S.-Q.; Kamachi, T.; Yao, Z.-S.; Huang, Y.-G.; Shiota, Y.; Yoshizawa, K.; Azuma, N.; Miyazaki, Y.; Nakano, M.; Maruta, G.; Takeda, S.; Kang, S.; Kanegawa, S.; Sato, O. Assembling an Alkyl Rotor to Access Abrupt and Reversible Crystalline Deformation of a Cobalt(II) Complex. *Nat. Commun.* **2015**, *6* (1), 8810.
(54) Juhász, G.; Matsuda, R.; Kanegawa, S.; Inoue, K.; Sato, O.; Yoshizawa, K. Bistability of Magnetization without Spin-Transition in a High-Spin Cobalt(II) Complex Due to Angular Momentum Quenching. *J. Am. Chem. Soc.* **2009**, *131* (13), 4560−4561.
(55) Yamada, M.; Fukumoto, E.; Ooidemizu, M.; Bréfuel, N.; Matsumoto, N.; Iijima, S.; Kojima, M.; Re, N.; Dahan, F.; Tuchagues, J.-P. A 2D Layered Spin Crossover Complex Constructed by NH···Cl^- Hydrogen Bonds: $[Fe^{II}H_3L^{Me}]Cl{\cdot}I_3$ (H_3L^{Me} = Tris[2-(((2-methylimidazoyl-4-yl)methylidene)amino)ethyl]amine. *Inorg. Chem.* **2005**, *44* (20), 6967−6974.
(56) Hagiwara, H.; Matsumoto, N.; Iijima, S.; Kojima, M. Layered Iron(II) Spin Crossover Complex Constructed by NH···Br^- Hydrogen Bonds with 2 K Wide Thermal Hysteresis, $[Fe^{II}H_3L^{Me}]Br{\cdot}CF_3SO_3$ (H_3L^{Me} = Tris[2-(((2-methylimidazol-4-yl)methylidene)-amino)ethyl]-amine). *Inorg. Chim. Acta* **2011**, *366* (1), 283−289.
(57) Ikuta, Y.; Ooidemizu, M.; Yamahata, Y.; Yamada, M.; Osa, S.; Matsumoto, N.; Iijima, S.; Sunatsuki, Y.; Kojima, M.; Dahan, F.; Tuchagues, J.-P. A New Family of Spin Crossover Complexes with a Tripod Ligand Containing Three Imidazoles: Synthesis, Characterization, and Magnetic Properties of $[Fe^{II}H_3L^{Me}](NO_3)_2{\cdot}1.5H_2O$, $[Fe^{III}L^{Me}]{\cdot}3.5H_2O$, $[Fe^{II}H_3L^{Me}][Fe^{II}L^{Me}]NO_3$, and $[Fe^{II}H_3L^{Me}][Fe^{III}L^{Me}](NO_3)_2$ (H_3L^{Me} = Tris[2-(((2-methylimidazol-4-yl)methylidene)amino)ethyl]amine). *Inorg. Chem.* **2003**, *42* (22), 7001−7017.
(58) Bréfuel, N.; Collet, E.; Watanabe, H.; Kojima, M.; Matsumoto, N.; Toupet, L.; Tanaka, K.; Tuchagues, J.-P. Nanoscale Self-Hosting of Molecular Spin-States in the Intermediate Phase of a Spin-Crossover Material. *Chem. - Eur. J.* **2010**, *16* (47), 14060−14068.

https://dx.doi.org/10.1021/acs.inorgchem.0c01069
Inorg. Chem. XXXX, XXX, XXX−XXX

(59) Westre, T. E.; Kennepohl, P.; DeWitt, J. G.; Hedman, B.; Hodgson, K. O.; Solomon, E. I. A Multiplet Analysis of Fe K-Edge 1s → 3d Pre-Edge Features of Iron Complexes. *J. Am. Chem. Soc.* **1997**, *119* (27), 6297−6314.
(60) Létard, J.-F. Photomagnetism of Iron(II) Spin Crossover Complexes—the *T*(LIESST) Approach. *J. Mater. Chem.* **2006**, *16* (26), 2550−2559.
(61) Létard, J.-F.; Guionneau, P.; Nguyen, O.; Costa, J. S.; Marcén, S.; Chastanet, G.; Marchivie, M.; Goux-Capes, L. A Guideline to the Design of Molecular-Based Materials with Long-Lived Photomagnetic Lifetimes. *Chem. - Eur. J.* **2005**, *11* (16), 4582−4589.
(62) Frisch, M. J.; Trucks, G. W.; Schlegel, H. B.; Scuseria, G. E.; Robb, M. A.; Cheeseman, J. R.; Scalmani, G.; Barone, V.; Mennucci, B.; Petersson, G. A.; Nakatsuji, H.; Caricato, M.; Li, X.; Hratchian, H. P.; Izmaylov, A. F.; Bloino, J.; Zheng, G.; Sonnenberg, J. L.; Hada, M.; Ehara, M.; Toyota, K.; Fukuda, R.; Hasegawa, J.; Ishida, M.; Nakajima, T.; Honda, Y.; Kitao, O.; Nakai, H.; Vreven, T.; Montgomery, J. A., Jr.; Peralta, J. E.; Ogliaro, F.; Bearpark, M.; Heyd, J. J.; Brothers, E.; Kudin, K. N.; Staroverov, V. N.; Keith, T.; Kobayashi, R.; Normand, J.; Raghavachari, K.; Rendell, A.; Burant, J. C.; Iyengar, S. S.; Tomasi, J.; Cossi, M.; Rega, N.; Millam, J. M.; Klene, M.; Knox, J. E.; Cross, J. B.; Bakken, V.; Adamo, C.; Jaramillo, J.; Gomperts, R.; Stratmann, R. E.; Yazyev, O.; Austin, A. J.; Cammi, R.; Pomelli, C.; Ochterski, J. W.; Martin, R. L.; Morokuma, K.; Zakrzewski, V. G.; Voth, G. A.; Salvador, P.; Dannenberg, J. J.; Dapprich, S.; Daniels, A. D.; Farkas, O.; Foresman, J. B.; Ortiz, J. V.; Cioslowski, J.; Fox, D. J. *Gaussian 09*, Revision B.01; Gaussian, Inc.: Wallingford, CT, 2010.
(63) Cirera, J.; Via-Nadal, M.; Ruiz, E. Benchmarking Density Functional Methods for Calculation of State Energies of First Row Spin-Crossover Molecules. *Inorg. Chem.* **2018**, *57* (22), 14097−14105.

https://dx.doi.org/10.1021/acs.inorgchem.0c01069
Inorg. Chem. XXXX, XXX, XXX−XXX